
Since January 2020 Elsevier has created a COVID-19 resource centre with free information in English and Mandarin on the novel coronavirus COVID-19. The COVID-19 resource centre is hosted on Elsevier Connect, the company's public news and information website.

Cell Reports

Article

# A two-adjuvant multiantigen candidate vaccine induces superior protective immune responses against SARS-CoV-2 challenge

## Graphical abstract

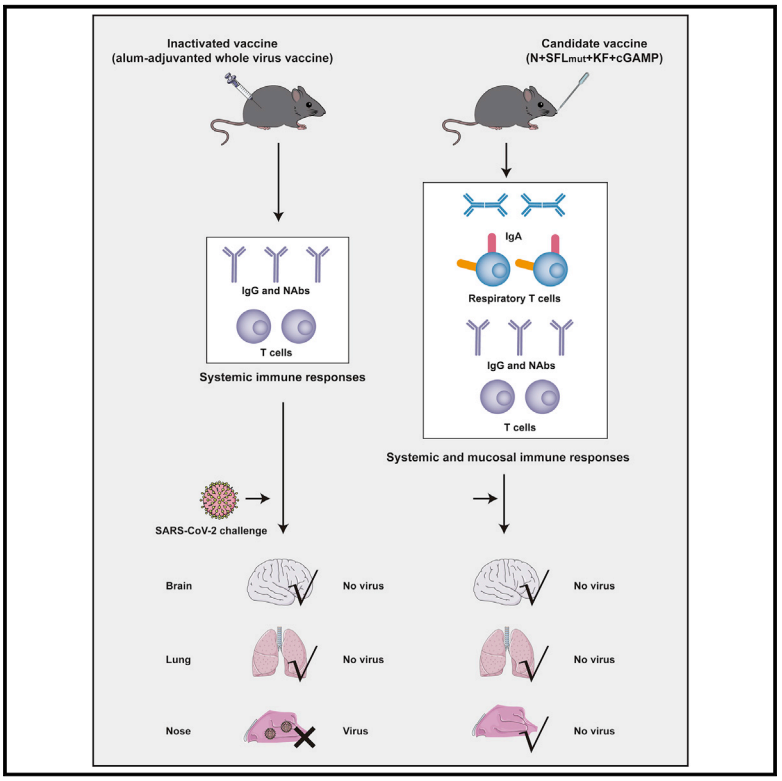


## Highlights

- A two-adjuvant multiantigen candidate vaccine induces a multifaceted immune response
- A candidate vaccine protects hACE2 transgenic mice from lethal SARS-CoV-2 challenge
- Intranasal delivery of candidate vaccine shows superior protection in the URT
- A candidate vaccine induces cross-reactive T cells against SARS-CoV-2 variants

## Authors

Wenwen Jiang, Li Shi, Lukui Cai, ..., Jing Li, Longding Liu, Mingbo Sun

## Correspondence

longdingl@gmail.com (L.L.), smb@imbcams.com.cn (M.S.)

## In brief

Jiang et al. show that a candidate vaccine, comprising the N and $SFL_{mut}$ proteins adjuvanted with KF and cGAMP, induces strong systemic and mucosal immune responses and protects hACE2 transgenic mice from a lethal SARS-CoV-2 challenge with robust viral clearance in the upper respiratory tract compared with a reference inactivated vaccine.

Jiang et al., 2021, Cell Reports *37*, 110112
December 14, 2021 
https://doi.org/10.1016/j.celrep.2021.110112

CellPress

Cell Reports

CellPress
OPEN ACCESS

Article

# A two-adjuvant multiantigen candidate vaccine induces superior protective immune responses against SARS-CoV-2 challenge

Wenwen Jiang,[1,5] Li Shi,[2,5] Lukui Cai,[3,5] Xiaoyu Wang,[1] Jingyan Li,[3] Heng Li,[4] Jiangli Liang,[1] Qin Gu,[1] Guang Ji,[3] Jing Li,[4] Longding Liu,[4,*] and Mingbo Sun[1,3,6,*]

[1]Yunnan Key Laboratory of Vaccine Research and Development on Severe Infectious Diseases, Institute of Medical Biology, Chinese Academy of Medical Science & Peking Union Medical College, Kunming, Yunnan, China

[2]Laboratory of Immunogenetics, Institute of Medical Biology, Chinese Academy of Medical Science & Peking Union Medical College, Kunming, Yunnan, China

[3]Laboratory of Vaccine Development, Institute of Medical Biology, Chinese Academy of Medical Science & Peking Union Medical College, Kunming, Yunnan, China

[4]Laboratory of Respiratory Infection, Kunming National High-level Biosafety Research Center, Institute of Medical Biology, Chinese Academy of Medical Science & Peking Union Medical College, Kunming, Yunnan, China

[5]These authors contributed equally

[6]Lead contact

*Correspondence: longdingl@gmail.com (L.L.), smb@imbcams.com.cn (M.S.)

https://doi.org/10.1016/j.celrep.2021.110112

## SUMMARY

An ideal vaccine against SARS-CoV-2 is expected to elicit broad immunity to prevent viral infection and disease, with efficient viral clearance in the upper respiratory tract (URT). Here, the N protein and prefusion-full S protein ($SFL_{mut}$) are combined with flagellin (KF) and cyclic GMP-AMP (cGAMP) to generate a candidate vaccine, and this vaccine elicits stronger systemic and mucosal humoral immunity than vaccines containing other forms of the S protein. Furthermore, the candidate vaccine administered via intranasal route can enhance local immune responses in the respiratory tract. Importantly, human ACE2 transgenic mice given the candidate vaccine are protected against lethal SARS-CoV-2 challenge, with superior protection in the URT compared with that in mice immunized with an inactivated vaccine. In summary, the developed vaccine can elicit a multifaceted immune response and induce robust viral clearance in the URT, which makes it a potential vaccine for preventing disease and infection of SARS-CoV-2.

## INTRODUCTION

Since the emergence of severe acute respiratory syndrome coronavirus 2 (SARS-CoV-2), this virus has spread worldwide, causing the ongoing coronavirus disease 2019 (COVID-19) pandemic, which has resulted in over two million deaths (https://covid.cdc.gov/covid-data-tracker/#global-counts-rates). Developing a vaccine that can not only prevent COVID-19 but also stop the transmission of SARS-CoV-2, especially with the ability to clear the virus in the upper respiratory tract (URT), is the major target of vaccine developers. Numerous vaccines are being developed to control this disease, with development at different stages ranging from preclinical studies and phase I–III trials to launch in the marketplace for emergency use (Krammer, 2020; Polack et al., 2020; Ramasamy et al., 2021). Given the knowledge on SARS-CoV-2 infection and the associated pathogenic mechanism, as well as safety considerations, major efforts in SARS-CoV-2 vaccine development are devoted to investigating protein subunit vaccine candidates containing viral components such as the SARS-CoV-2 spike (S) protein and its derivatives, S1 protein, receptor-binding domain (RBD), and nucleocapsid (N) protein. Most of these vaccines are virus based or mRNA based and employ the S protein, which is considered the critical antigen for inducing protective host immunity (Lurie et al., 2020; Walls et al., 2020; Yang et al., 2020).

The full-length SARS-CoV-2 S ($S_{CoV-2}$) protein contains 1,273 aa and consists of the S1 and S2 subunits. In the S1 subunit, there is an RBD, which is considered the primary target of neutralizing antibodies (NAbs) (Barnes et al., 2020; Huang et al., 2020; Yang et al., 2020). The highly glycosylated $S_{CoV-2}$ protein forms homotrimeric spikes on the virion and mediates SARS-CoV-2 receptor binding through angiotensin-converting enzyme 2 (ACE2) to promote virus entry into host cells (Letko et al., 2020). As the virus enters through the host cell membrane, the S protein undergoes structural changes. This process involves the binding of the S1 subunit of the virus to the host cell receptor, triggering the occurrence of trimer instability, which in turn causes the S1 subunit to dissociate from the S2 subunit and the S2 subunit to form a highly stable fused structure. To bind to host cell receptors, the RBD of S1 undergoes a hinge-like fusion conformational movement to transiently hide or expose the key sites in the RBD. These two states are referred

to as the "down" and "up" conformations, where "down" corresponds to the receptor-inaccessible state and "up" corresponds to the receptor-accessible state; the "up" state is considered relatively unstable (Fan et al., 2020). Thus, a $S_{CoV-2}$ construct that remains in the "up" state could be a promising candidate component for vaccination aimed at eliciting NAbs (Henderson et al., 2020; Secchi et al., 2020).

Although the majority of vaccines in development are focused on the S protein, the SARS-CoV-2 N protein has also been proposed as a promising vaccine component (Dutta et al., 2020). Studies have shown that the N protein of SARS-CoV-2 can elicit strong humoral and cellular immunity (Ferretti et al., 2020; He et al., 2021; Ni et al., 2020). Notably, a recent study by Dangi et al. (2021) found that a spike-based vaccine does not provide acute protection to the central nervous system; however, only when co-administered with a spike-based vaccine and a nucleocapsid-based vaccine, protection against distal viral dissemination to the nervous system was observed. Moreover, the emergence of more transmissible SARS-CoV-2 variants including B.1.351 (Beta) and B.1.617.2 (Delta) with mutations in the spike protein are potentially capable of evading vaccination-induced NAbs and result in a growing number of breakthrough infections (Bian et al., 2021; Karim, 2021; Prévost and Finzi, 2021; Wang et al., 2021b). In contrast, the N protein is more conserved than the S protein, and this characteristic is likely to induce an immune response against SARS-CoVs in future outbreaks, which makes the N protein an important vaccine target (Oliveira et al., 2020). Therefore, including the N protein in a SARS-CoV-2 vaccine can not only increase immunogenicity and protective efficacy but also ensure a potential variant-proof vaccine for use in the future, which is exactly the multiantigen strategy in the current study based on.

Some SARS-CoV-2 vaccines are currently being used in the clinic, and multiple vaccines are in clinical trials (Krammer, 2020; Polack et al., 2020; Ramasamy et al., 2021); these vaccines can elicit strong humoral and/or cellular immune responses against the virus, but their activity against infection, in terms of stopping virus transmission and reducing the entire population's overall exposure to the virus, is not completely satisfactory (Gao et al., 2020; van Doremalen et al., 2020; Yu et al., 2020). In contrast to systemic responses, efficient mucosal immunity, including immunity mediated by secretory immunoglobulin A (IgA) and tissue-resident memory T (TRM) cells, can prevent and terminate viral infections of the URT in the early phase, and this phenomenon can effectively prevent lower respiratory tract viral infections and further prevent the spread of disease. However, inducing effective specific IgA and T cell responses in the mucosa requires the use of appropriate adjuvants. Here, we investigated the combination of flagellin (KF) plus cyclic GMP-AMP (cGAMP) as a combined adjuvant for SARS-CoV-2 mucosal peptide vaccines. Flagellin, a principal component of bacterial flagella, affects both innate and adaptive immune responses via the TLR5 signaling pathway (Honko and Mizel, 2005). Many studies have shown that flagellin is a potent mucosal adjuvant that enhances the B cell transition to IgA-secreting cells and promotes specific mucosal T cell responses (Flores-Langarica et al., 2012; Mizel and Bates, 2010). cGAMP, the major ligand of stimulator of interferon genes (STINGa), can activate the TANK-binding kinase 1 (TBK-1)-IRF-3 axis and thus induce the expression of type I interferons (IFN-I) (Burdette et al., 2011; Burdette and Vance, 2013). cGAMP has been reported to function as a mucosal adjuvant against respiratory pathogen infection, including infection with influenza, anthrax, *Streptococcus pneumoniae*, *Klebsiella pneumoniae*, and *Mycobacterium tuberculosis* (Blaauboer et al., 2015; Karaolis et al., 2007; Luo et al., 2019; Martin et al., 2017). Although previous reports have indicated the potential of flagellin and cGAMP to function as separate adjuvants for mucosal vaccines and studies have shown that cGAMP can synergize with TLR agonists to promote immune responses (Temizoz et al., 2018), no studies have investigated whether the combination of these two reagents can strengthen mucosal adjuvant effects.

In this study, we first tested the synergistic adjuvant effects of nonpathogenic *Escherichia coli*-derived flagellin (KF) and cGAMP *in vivo* and *in vitro* by using bone marrow-derived dendritic cells (BMDCs) and the model antigen ovalbumin (OVA). Subsequently, we evaluated the optimal forms of the S protein for use as an antigen. Finally, we prepared a multiantigen-based SARS-CoV-2 vaccine formulated with this combined adjuvant and then compared its immunogenicity and protective efficacy with those of a reference inactivated vaccine in mouse models. We aimed to search for a candidate vaccine that has the potential to elicit humoral, cellular, and mucosal immunity to prevent viral infection and disease and to promote efficient viral clearance from the URT.

## RESULTS

### KF and cGAMP synergistically promoted maturation of BMDCs and enhanced mucosal immune responses

To assess the activation of $CD11c^+$ BMDCs by KF, cGAMP, or KF plus cGAMP, flow cytometry was used to measure the cell-surface expression of major histocompatibility complex molecule class II (MHC II) and the costimulatory molecules CD86, CD80, and CD40. Significant upregulation of MHC II expression was observed on BMDCs cultured with KF plus cGAMP compared to BMDCs cultured with the individual adjuvant components (Figures 1A and 1B). Moreover, the expression of the costimulatory molecules CD86, CD80, and CD40 in the KF plus cGAMP group was also significantly higher than that in the single component groups (Figures 1A and 1B). Additionally, the levels of interferon-β (IFN-β), IP-10, tumor necrosis factor-α (TNF-α), and interleukin-6 (IL-6) were measured in the supernatants of BMDC cultures. Compared with the individual components, KF plus cGAMP promoted BMDC secretion of IP-10, TNF-α, and IL-6 (Figure S1A). The presence of IFN-β in the culture supernatant was below the limits of detection when BMDCs were stimulated with either PBS or KF, but it was detectable when BMDCs were stimulated with cGAMP or KF plus cGAMP, and there were no differences between these two groups (Figure S1A). Taken together, these results indicated that the combination of KF and cGAMP was able to significantly promote the expression of surface markers that are involved in BMDC maturation and antigen presentation and enhance the secretion of cytokines from

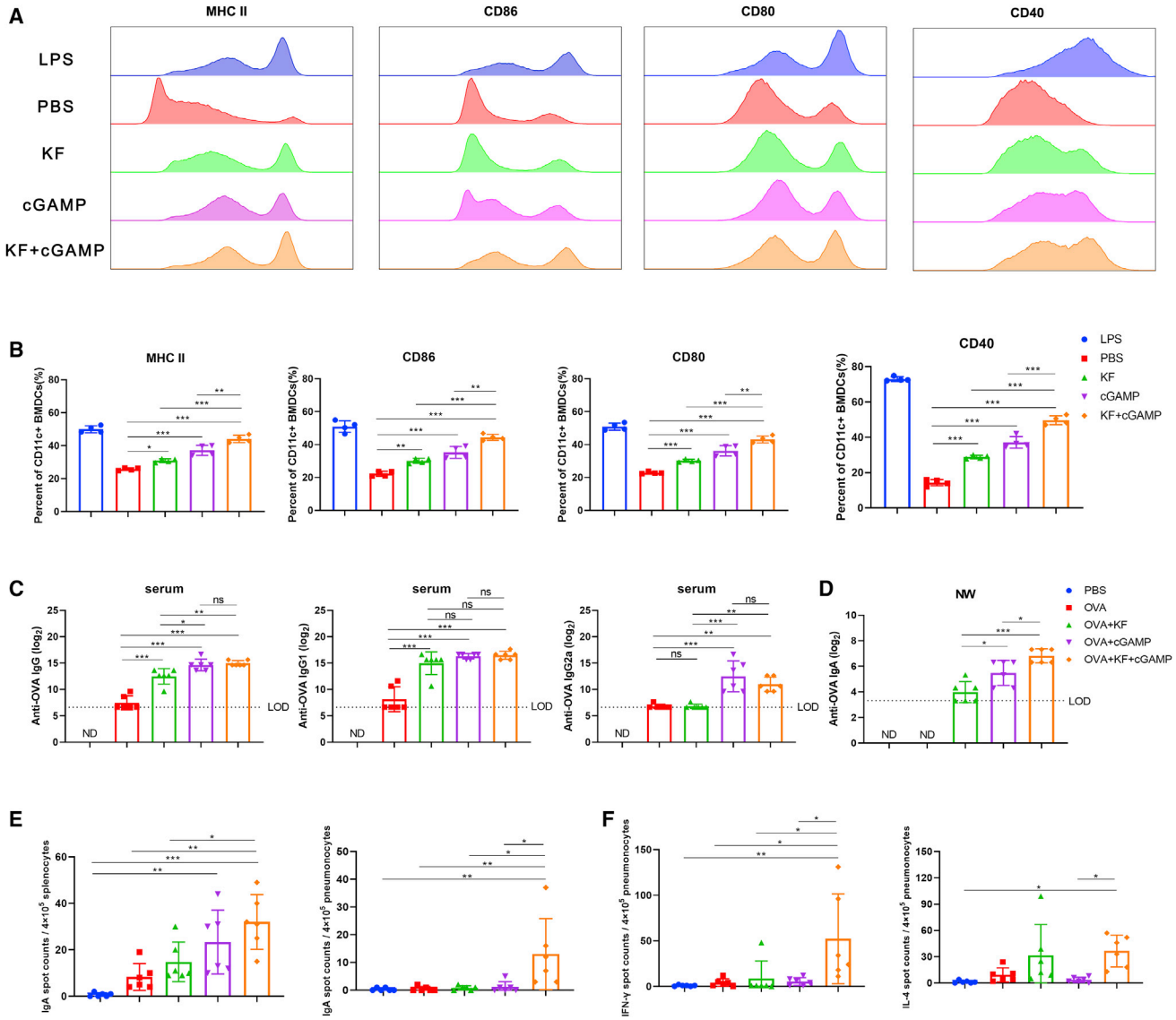


**Figure 1. KF and cGAMP synergistically promoted the maturation of BMDCs and enhanced mucosal immune responses**

(A and B) BMDCs were stimulated with KF (4 μg/mL), cGAMP (4 μg/mL), or KF (4 μg/mL) plus cGAMP (4 μg/mL) *in vitro* for 24 h. The cells were treated with lipopolysaccharide (LPS, 1 μg/mL) or sterile PBS as positive and negative controls, respectively. BMDCs were harvested and analyzed via flow cytometry to determine the surface expression of MHC II, CD86, CD80, or CD40. The data are expressed as the mean ± the SEM of four independent experiments.

(C) Mice were intranasally administered OVA alone or adjuvanted with KF, cGAMP, or KF plus cGAMP three times at 2-week intervals and euthanized on day 14 after the last immunization. PBS-immunized mice served as negative controls. Serum was collected for the determination of IgG, IgG1, and IgG2a responses (n = 6 mice per group).

(D) Nasal washes (NW) were collected for the detection of OVA-specific IgA antibodies (n = 6 mice per group).

(E) Lung and spleen tissues were harvested for the detection of OVA-specific IgA-secreting cells by ELISpot assay (n = 6 mice per group).

(F) Lung tissues were assayed by ELISpot to assess specific IFN-γ and IL-4 production. Data are expressed as the mean ± the SEM (n = 6 mice per group). The dotted line indicates the limit of detection (LOD), and values that fell below the detection limit are represented by the limit of detection value for statistical analysis. "ND" indicates that no individuals in this group had detectable levels. Significance was determined via one-way ANOVA with a Tukey multiple comparison test. *p < 0.05, **p < 0.01, ***p < 0.001, ns, no significance. See also Figure S1.

dendritic cells, which possibly play a better role in immune regulation.

To further evaluate whether the promotion of BMDC function by the combined adjuvant could translate to enhanced adjuvant effects *in vivo*, mice were intranasally immunized with OVA coadministered with KF, cGAMP, or KF plus cGAMP on days 0, 14, and 28. The immunoglobulin levels in the sera on day 14 after the last immunization indicated that KF, cGAMP, or KF plus cGAMP induced significantly higher anti-OVA IgG antibodies production than OVA alone (Figure 1C). KF predominantly

induced the production of IgG1 in a Th2-type response, and cGAMP, alone or in combination with KF, induced the production of both IgG1 and IgG2a in a more balanced Th1-Th2-type response (Figure 1C). In addition, we measured the anti-OVA IgA antibodies in bronchoalveolar lavage fluid (BALF) and nasal wash (NW). Specifically, animals that received OVA adjuvanted with KF plus cGAMP had higher levels of OVA-specific IgA antibodies in their NW compared to animals that received OVA alone or OVA admixed with a single adjuvant (Figure 1D). Interestingly, low levels of anti-OVA IgA antibodies were only observed in the BALF of animals given OVA adjuvanted with KF plus cGAMP, and mice receiving OVA alone or OVA supplemented with individual adjuvants failed to produce detectable anti-OVA IgA levels in the BALF (Figure S1B). Notably, consistent with these anti-OVA IgA antibody responses, the numbers of splenic and pulmonary IgA-secreting cells were significantly increased in animals given the OVA adjuvant with KF plus cGAMP (Figure 1E). Furthermore, we measured the presence of IFN-$\gamma^+$ and IL-4$^+$ splenocytes and pneumonocytes using an ELISpot assay. The results indicated that cGAMP significantly increased the numbers of OVA-specific IFN-$\gamma$- and IL-4-secreting T cells in splenocytes (Figure S1C). However, the combination of KF and cGAMP markedly increased the numbers of IFN-$\gamma$- and IL-4-secreting T cells in lung tissues (Figure 1F). Together, the data suggest that KF plus cGAMP may be a more potent enhancer of mucosal immune responses.

## $SFL_{mut}$ induces potent NAbs and mucosal immunity compared with other forms of the S protein

To determine the optimal S protein-associated antigens able to induce NAbs against SARS-CoV-2, we evaluated experimental vaccines harboring the N protein with different S protein-associated antigens and the two adjuvants: (1) RBD, (2) S1 subunit (S1), (3) full-length S protein (SFL), and (4) the prefusion S-protein structure generated by mutating eight amino acid sites ($SFL_{mut}$) (Hsieh et al., 2020); all of the S protein-associated antigens contained the RBD. Two weeks after the third immunization, the S protein-specific IgG and IgA levels in mouse serum, BALF, and NW were determined (Figure 2A). In the serum, the titers of IgG specific for the purified S protein and whole virus in the SFL and $SFL_{mut,}$ groups were higher than those in the RBD and S1 groups, but differences were not found between the SFL and $SFL_{mut,}$ groups (Figures 2B and 2C). The $SFL_{mut}$ group exhibited higher anti-RBD IgG titers than the S1 and SFL groups but did not exhibit a difference from the RBD group (Figure 2B). Moreover, NAbs were induced only in the $SFL_{mut}$ group and in 50% of the mice in the RBD group (Figure 2D). These results suggest that the conformation of $SFL_{mut}$ may preserve relevant B cell epitopes, which are likely hidden in the S1 subunit and SFL, and exposure of these epitopes could be crucial for production of NAbs.

We also assessed the antibody responses in the NW and BALF of mice. NW samples from SFL and $SFL_{mut}$ mice, but not those from S1 and RBD mice, showed high levels of anti-S protein IgA antibodies (Figure 2E). High RBD-specific IgA titers in both the NW and the BALF were measured in $SFL_{mut}$ mice and were significantly higher than those in all the other groups (Figures 2E and 2F). Unexpectedly, there were low S-specific IgA titers in the BALF of all mice (Figure 2F); however, the RBD-specific IgA titers in the BALF of $SFL_{mut}$ mice were higher than those of the mice in other groups. All these data indicated that mice immunized with $SFL_{mut}$ showed more potent mucosal and systemic humoral immunity than those immunized with the other experimental vaccines. Therefore, we selected $SFL_{mut}$ as the ideal antigen of candidate vaccine to further explore the cellular and mucosal immunity and its protective efficacy.

## Intranasal administration of the candidate vaccine drives strong systemic and mucosal immune responses

To further determine whether KF plus cGAMP induces systemic and local mucosal immune responses to the SARS-CoV-2 peptide vaccine, mice were given $SFL_{mut}$ and N proteins supplemented with or without the combined adjuvant via the intranasal route (i.n.) three times at 2-week intervals. These groups were compared to a reference vaccine that is known to be protective: an inactivated whole-virus vaccine administered intraperitoneally (i.p.) in mice two times at 4-week intervals in preclinical experiments. Additionally, to determine whether the effects of the combined adjuvant were dependent on the immunization route, mice were immunized with $SFL_{mut}$ and N proteins combined with KF and cGAMP via the i.p. route. Mice in the i.n. group were administered PBS as a placebo (Figure 3A).

Specific anti-S, anti-RBD, and anti-N IgG antibodies were detected, and the antigen-only group showed minimal IgG antibody levels (Figures 3B and 3C). The serum anti-S and anti-RBD IgG antibody levels were similar between the mice immunized with $N^+SFL_{mut}{}^+KF^+$cGAMP (i.n.) and those immunized with $N^+SFL_{mut}{}^+KF^+$cGAMP (i.p.) (Figure 3B), but i.p. immunization resulted in a significant increase in anti-N protein IgG titers (Figure 3C). However, no significant differences were observed between the $N^+SFL_{mut}{}^+KF^+$cGAMP (i.n.) and the inactivated vaccine (Figures 3B and 3C). In addition, we measured the presence of IgA antibodies in the BALF and NW, and antigen-specific IgA antibodies were not detectable in the $N^+SFL_{mut}$-only group or in the group immunized via the i.p. route. The $N^+SFL_{mut}{}^+KF^+$cGAMP (i.n.) group exhibited a high response with specific anti-S and anti-RBD IgA titers in the BALF and NW, suggesting the potential for improved IgA antibodies production with the combined adjuvant (Figure S2). Antigen-specific T cell responses in splenocytes and lung tissues were then assessed via ELISpot assay. Low overall numbers of IFN-$\gamma$- and IL-4-secreting T cells were observed in both the spleen and lung tissues of the antigen-only group (Figures 3D and 3E). In contrast, $N^+SFL_{mut}{}^+KF^+$cGAMP administered via the i.n. or i.p. route induced magnified T cell responses in splenocytes (Figure 3D); however, i.n. immunization resulted in a significant increase in T cell responses in lung tissues (Figure 3E). Similarly, we observed robust cellular immune responses in the splenocytes from mice given the $N^+SFL_{mut}{}^+KF^+$cGAMP via the i.n. route and the inactivated vaccine via the i.p. route; however, pneumonocyte T cell responses were stronger in the $N^+SFL_{mut}{}^+KF^+$cGAMP i.n. group than the inactivated vaccine group (Figures 3D and 3E). Together, these results indicated that $N^+SFL_{mut}{}^+KF^+$cGAMP administered via the i.n. route could be an appropriate candidate mucosal vaccine for SARS-CoV-2.

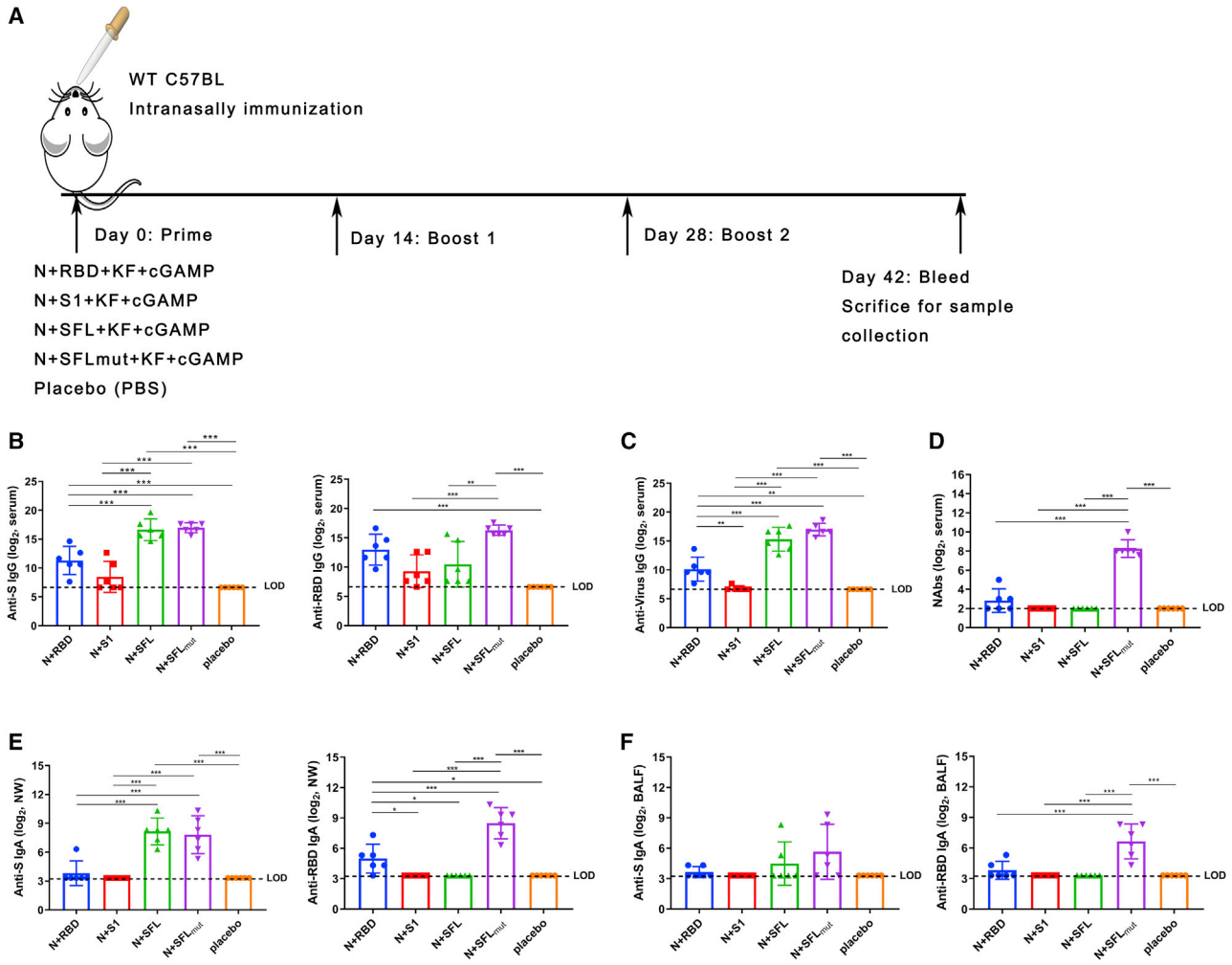


**Figure 2. Induction of antibody responses by experimental vaccines**

(A) Diagram of C57BL/6 mouse immunization. Six- to 8-week-old C57BL/6 mice were immunized with three doses of experimental vaccines (the N protein and one of the following S protein-associated antigens: (1) the RBD (RBD), (2) the S1 subunit (S1), (3) the full-length S protein (SFL), or (4) the prefusion S protein structure generated by mutating eight amino acid sites ($SFL_{mut}$)) via the intranasal route at 14-day intervals. Two weeks after the third immunization, the mice were sacrificed, and antibody responses in the serum, nasal wash (NW), and bronchoalveolar lavage fluid (BALF) were evaluated.

(B and C) Humoral immune responses in the serum were evaluated using S protein-, RBD-, N protein-, or inactivated SARS-CoV-2- based IgG ELISA on day 14 after the third immunization (n = 6 mice per group).

(D) Neutralizing antibodies (NAbs) in the serum were evaluated by a SARS-CoV-2 neutralization assay in a BSL-3 laboratory (n = 6 mice per group).

(E) Mucosal immune responses in the NW were evaluated using S protein- or RBD protein-based IgA ELISA on day 14 after the third immunization (n = 6 mice per group).

(F) Mucosal immune responses in the BALF were evaluated using S protein- or RBD-based IgA ELISA on day 14 after the third immunization (n = 6 mice per group). Data are expressed as the mean ± the SEM. The dotted line indicates the limit of detection (LOD), and values that fell below the detection limit are represented by the limit of detection value for statistical analysis. Significance was determined via one-way ANOVA with a Tukey multiple comparison test. *$p < 0.05$, **$p < 0.01$, ***$p < 0.001$.

To further assess whether the candidate vaccine could support local inductive responses, we harvested NALT from the animals at the time of euthanasia and performed flow-cytometric analysis. Compared with the inactivate vaccine and placebo groups, the candidate vaccine group showed robust increases in the frequencies of $CD8^+$ T cells and $IgA^+$ B cells (Figure 3F). Moreover, the TRM cell population, both the numbers of $CD4^+$ TRM cells and $CD8^+$ TRM cells in the lungs (the TRM cells gating strategy is shown in Figure S3), which were identified based on the $CD44^+CD62L^-CD69^+$ phenotype, were significantly higher in the candidate vaccine group than in the inactivated vaccine group and placebo group (Figure 3G).

## Intranasal immunization with the candidate vaccine upregulates mRNAs related to immune responses in C57BL/6 mice

The nasal mucosal and NALT were collected from C57BL/6 mice at 14 days after the last immunization to analyze the

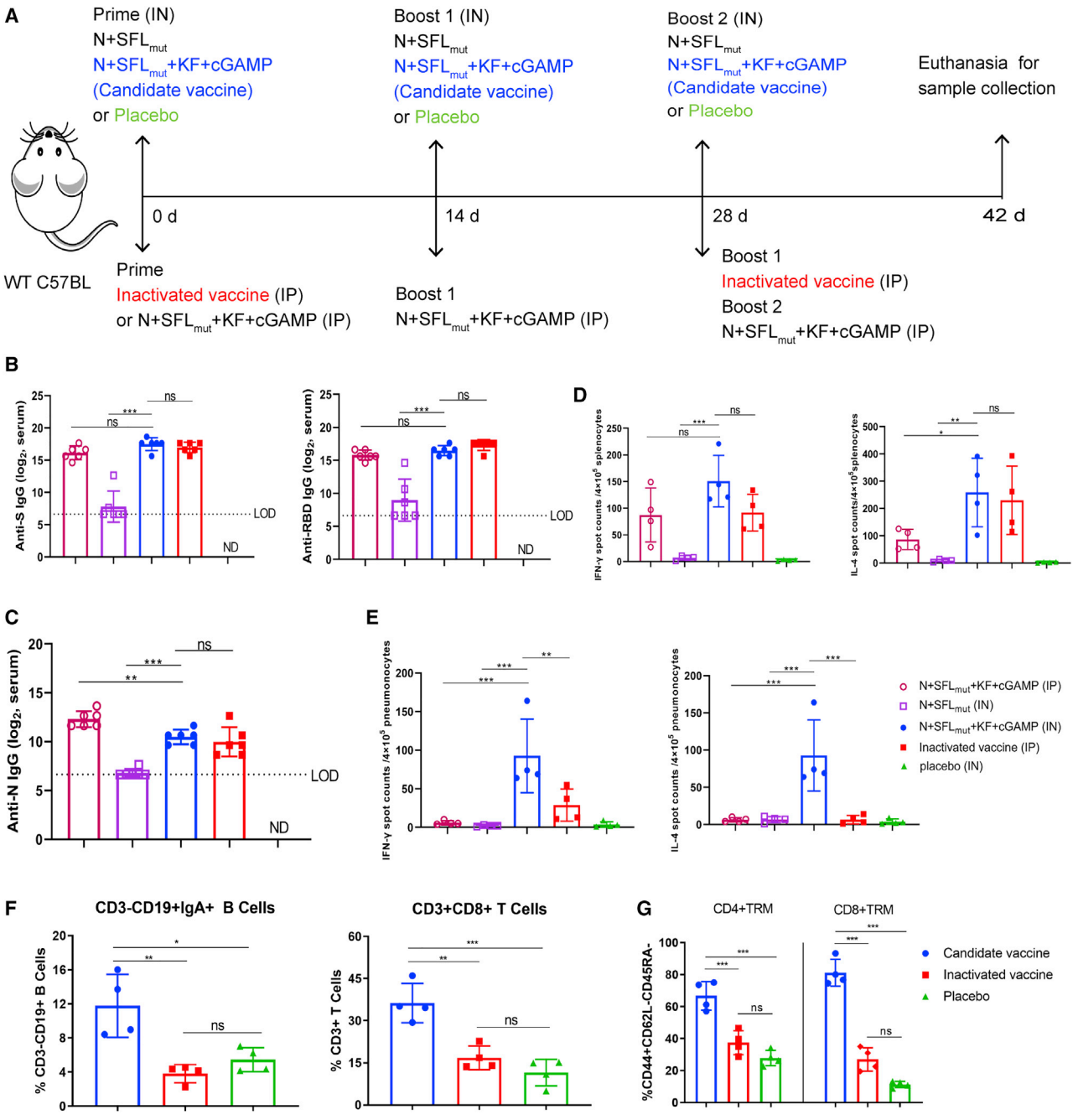


**Figure 3. Intranasal administration of the candidate vaccine drives strong systemic and mucosal immune responses**

C57BL/6 mice were given the SFL$_{mut}$ and N proteins supplemented with or without combined adjuvant via the intranasal route (i.n.) or immunized with the SFL$_{mut}$ and N proteins combined with KF and cGAMP via the i.p. route three times at 2-week intervals. These groups were compared to a group that received a reference inactivated vaccine via the intraperitoneal (i.p.) route twice at 4-week intervals. These mice were euthanized 14 days after the last immunization for sample collection.

(A) Vaccination scheme.

(B) Specific anti-S and anti-RBD IgG titers in serum (n = 6 mice per group).

(C) Specific anti-N IgG titers in serum (n = 6 mice per group).

(D) Splenocytes were assayed for IFN-γ and IL-4 cells production after re-stimulation with N and S protein by ELISpot assay (n = 4 mice per group).

(E) Lung tissues were assayed for IFN-γ and IL-4 cells production after re-stimulation with N and S protein by ELISpot assay (n = 4 mice per group).

(F and G) Nasal-associated lymphoid tissue (NALT) was collected from animals immunized with the candidate vaccine via the i.n. route, the inactivated vaccine via the i.p. route, and PBS via the i.n. route, and flow-cytometric analysis was performed. In addition, four mice in these three groups were intravenously (i.v.) injected with an anti-CD45 antibody 8 min prior to euthanasia. The lungs were collected, and lung mononuclear cells were stained with antibodies specific for CD3, CD4,

*(legend continued on next page)*

transcriptomic profile. On nasal mucosal RNA-sequencing (RNA-seq) analysis, 192 differentially expressed genes (DEGs) ($p \leq 0.05$, fold change >2.0) (142 upregulated and 50 downregulated) were exclusively found after intranasal immunization with the candidate vaccine compared with placebo vaccination. In contrast, only 1 DEG ($p \leq 0.05$, fold change >2.0) was identified when comparing the inactivated vaccine with the placebo (Figure 4A). To obtain more insight into the DEGs, functional annotation of GO-BP terms was performed with Metascape. Analysis of the 192 DEGs between the candidate vaccine- and placebo-vaccinated mice showed that 27 GO-BP terms were enriched, and the top 20 enriched GO terms are shown in Figure 4B. The enriched terms were mainly involved in the immune response, and we found that significant DEGs were involved in the responses to interferon (IFN), T cell activation, cell chemotaxis, and antigen processing and presentation of exogenous peptide antigen in mice immunized with the candidate vaccine. In addition, 22 and 13 genes were upregulated, and no genes were downregulated in the responses to interferon-gamma and interferon-beta GO-BP terms, respectively, in the candidate vaccine group compared with the placebo group (Figures 4C and 4D). Moreover, many specific cell chemotaxis (17 genes upregulated and one gene downregulated) terms changed (Figure 4E), which might be involved in the mucosal immune response to the candidate vaccine.

On NALT RNA-seq analysis, comparing the candidate vaccine-immunized mice with the placebo-immunized mice, 470 genes were differentially expressed ($p \leq 0.05$, fold change >2.0), with 322 upregulated and 148 downregulated. The top 20 enriched GO terms of the 64 GO-BP terms identified are shown in Figure S4A. Similar to the terms for the nasal mucosa, the dominant GO-BP terms were involved in immunity, but the major GO-BP terms included leukocyte proliferation, positive regulation of cytokine production, cell chemotaxis, and B cell proliferation. To further analyze the DEGs related to the GO-BP terms B cell proliferation (GO: 0042100) and cell chemotaxis (GO: 0060326), the specific DEGs were displayed in a heatmap (Figures S4B and S4C). The DEGs involved in the GO-BP term B cell proliferation (GO: 0042100) were all upregulated (Figure S4B). Elevated expression of mRNAs related to cell chemotaxis (GO: 0060326) in the NALT, particularly Spp1, Serpine1, and IL12a, was also observed in the nasal mucosa (Figure S4C). Taken together, our transcriptomic data further indicated that the candidate vaccine administered via intranasal immunization upregulated mRNA transcripts related to immune responses in the nasal mucosa and NALT, which might lead to enhanced local immune protection.

## Candidate vaccine protects hACE2 Tg mice from lethal SARS-CoV-2 challenge

6- to 8-week-old hACE2 Tg mice were immunized with three doses of the candidate vaccine or PBS via the intranasal route at 14-day intervals three times or primed via the intraperitoneal (i.p.) route with 100 U of inactivated SARS-CoV-2 vaccine and then boosted at 28 days with the same dose of the inactivated vaccine (Figure 5A). Serum samples were collected 7 days after the last immunization. Immunization with the candidate vaccine or inactivated vaccine but not immunization with the placebo control induced high levels of S-, RBD, and N- specific IgG antibodies (Figure 5B) and NAbs in the serum (Figure 5C). The candidate vaccine, not the inactivated vaccine, also induced high levels of S- and RBD-specific IgA antibodies in the serum (Figure 5D). At 10 days after the last vaccination, all mice were challenged intranasally with $10^3$ PFU of wild-type SARS-CoV-2, and all candidate vaccine- and inactivated vaccine-immunized mice survived this lethal challenge and lost little weight (Figures 5E and 5F). In contrast, the mice in the placebo group rapidly lost body weight beginning at 3 days post-infection (dpi), and these mice were humanely euthanized at 4 dpi (n = 4) or 5 dpi (n = 6) based on IMBCAMS-defined endpoints (Figures 5E and 5F). All these results indicate that the candidate vaccine can completely protect mice against lethal SARS-CoV-2 challenge as well as the inactivated vaccine.

## Intranasal immunization with the candidate vaccine prevents SARS-CoV-2 infection in the upper respiratory tract and tissues of hACE2 Tg mice

We first collected NW and throat swab samples from hACE2 Tg mice to evaluate dynamic viral load characteristics after SARS-CoV-2 challenge. Mice in the placebo group showed high copy numbers of viral RNA ($10^{6.07}$/100 μL) in the NW at 1 dpi, and the copy numbers remained at the same high levels until 4–5 dpi when the mice were humanly euthanized based on ethical endpoints (Figure 5A). As expected, inactivated vaccine-immunized animals treated via the intraperitoneal route also showed high copy numbers ($10^{5.49}$/100 μL) in the NW at 1 dpi, and the levels remained high until 4 dpi ($10^{5.45}$/100 μL), at which point a rapid decline was observed until the copy numbers were $10^{2.54}$/100 μL at 7 dpi (Figure 6A). In contrast, candidate vaccine-immunized mice treated intranasally showed very low viral RNA copy numbers, which were close to the limit of detection in the NW from 1 dpi to 4 dpi. Interestingly, the viral load increased slightly ($10^{3.67}$100 μL) at 5 dpi and then decreased rapidly to the detection limit at 7 dpi (Figure 6A). Viral RNA was detected in the throat swabs of the placebo group ($10^{3.76}$/100 μL) at 1 dpi, and the viral load continuously increased until the mice were humanly euthanized at 4–5 dpi (Figure 6B). For all vaccine-immunized mice, the dynamics of the viral load in throat swabs showed changes similar to those of the viral load in the NW (Figure 6B).

At 2, 5, and 7 dpi, the mouse brain, nasal turbinate, and lungs were monitored for viral replication. In placebo-immunized mice,

CD44, CD62L, and CD69 for flow-cytometric analysis. The results are expressed as $CD4^+$ TRM cells ($CD3^+CD4^+CD44^+CD62L^-CD45^-CD69^+$) and $CD8^+$ TRM cells ($CD3^+CD4^-CD44^+CD62L^-CD45^-CD69^+$). (F) NALT was assayed to determine the levels $CD3^+CD8^+$ T cells and $CD3^-CD19^+IgA^+$ B cells by flow cytometry (n = 4 mice per group). (G) $CD4^+$ TRM and $CD8^+$ TRM cells in the lungs. Representative flow cytometry gating strategies for $CD4^+$ TRM cells and $CD8^+$ TRM cells in the lungs are shown in Figure S3 (n = 4 mice per group). Data are expressed as the mean ± the SEM. The dotted line indicates the limit of detection (LOD), and values that fell below the detection limit are represented by the limit of detection value for statistical analysis. "ND" indicates that no individuals in this group had detectable levels. Significance was determined via one-way ANOVA with a Tukey multiple comparison test. *$p < 0.05$, **$p < 0.01$, ***$p < 0.001$, ns, no significance. See also Figures S2 and S3.

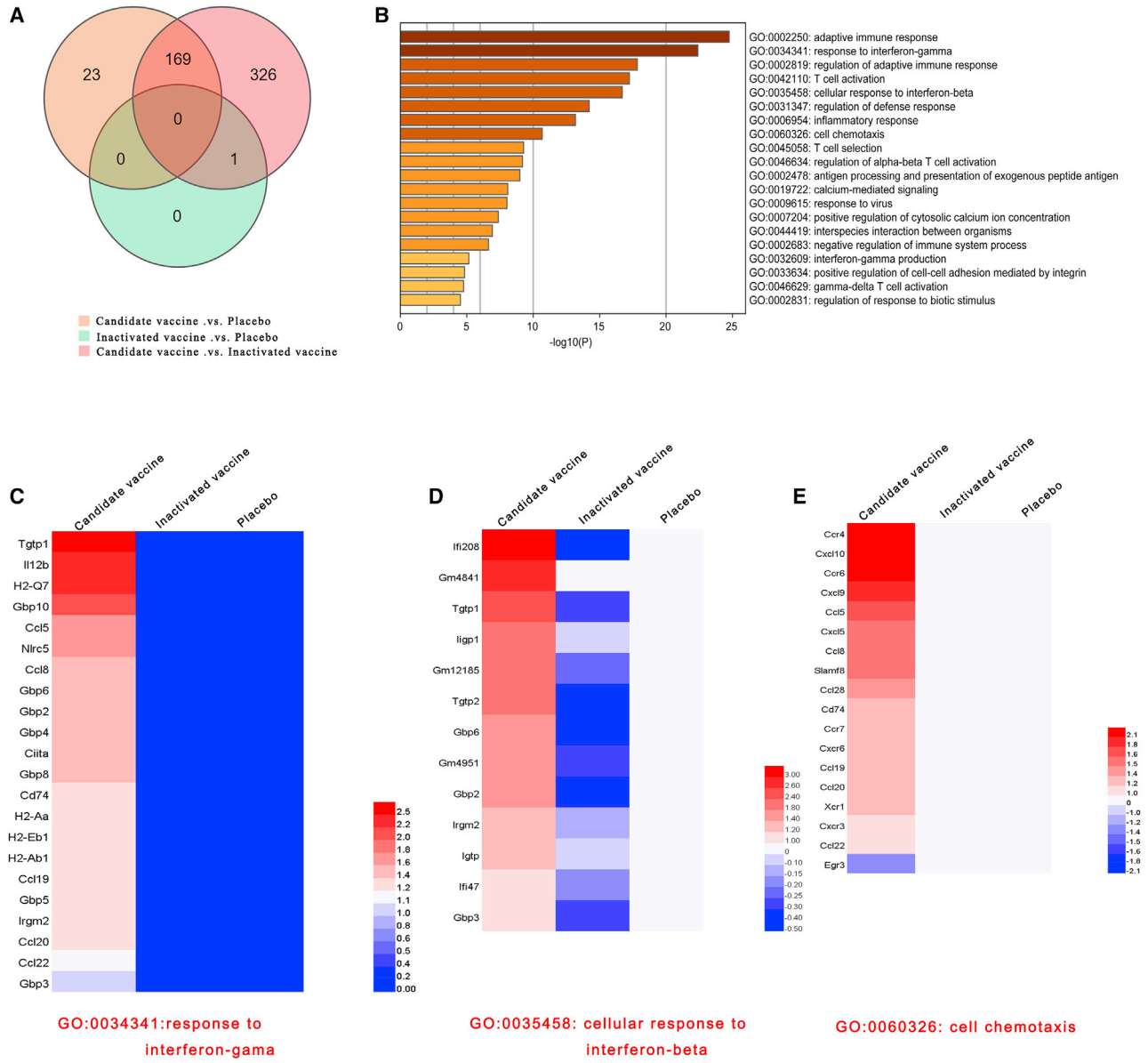


**Figure 4. mRNA expression profiles in mouse nasal mucosal samples collected on day 14 after the last immunization**

(A) A Venn diagram of RNA-seq data was used to illustrate the differentially expressed genes (DEGs) in the nasal mucosa among mice immunized with the candidate vaccine (n = 6 mice), inactivated vaccine (n = 6 mice), or placebo (n = 6 mice).

(B) Gene-enrichment analyses of the 470 DEGs. GO terms are labeled with the name and ID and were sorted by the –log10 (P) value.

(C) Heatmap of the 22 DEGs in the response to interferon-gamma term (GO: 0034341) among the three groups (n = 6 mice per group).

(D) Heatmap of the 13 DEGs in the cellular response to interferon-beta term (GO: 0035458) among the three groups (n = 6 mice per group).

(E) Heatmap of the 18 DEGs in the cell chemotaxis term (GO: 0060326) among the three groups (n = 6 mice per group). High-expression values are colored red, and low-expression values are colored blue. See also Figure S4.

the viral RNA copy number in the nasal turbinate increased from $1.38 \times 10^5$ copies/mg at 2 dpi to $1.74 \times 10^6$ copies/mg at 4/5 dpi (four mice were humanly euthanized at 4 dpi due to the IMBCAMS-defined endpoints, and the others were humanely euthanized at 5 dpi) (Figure 6C). Moreover, infectious virus was detected in the nasal turbinate, with the levels ranging from $1.35 \times 10^2$ CCID50/mL at 2 dpi to $7.92 \times 10^3$ CCID50/mL at 4 or 5 dpi (Figure 6C). In contrast, although low RNA copy numbers were detected in nasal turbinate, lung, and brain tissues, no infectious virus was detected in any of these tissues in the candidate vaccine group at the indicated times (Figures 6C–6E). Unexpectedly, 6.31 × 10 PFU/mL virus was detected in the nasal turbinate of one inactivated vaccine-immunized mouse (n = 4) at 2 dpi, but virus was not detected in the lungs or brain tissues (Figures 6C–6E). Live virus was not detected in any tissues in inactivated vaccine-immunized mice at 5 or 7 dpi (Figures 6C–6E).

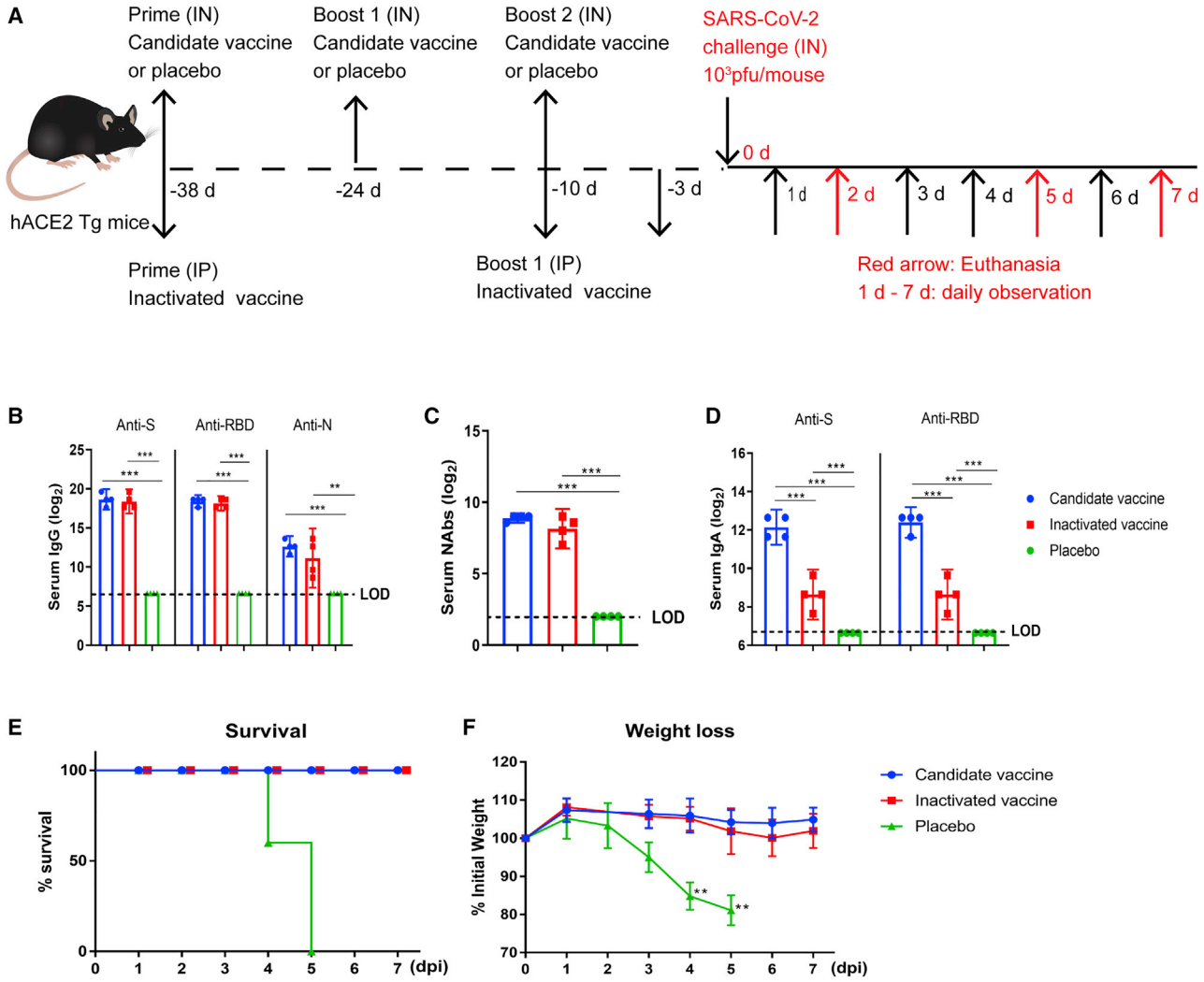


**Figure 5. Immunogenicity and protective efficacy of the candidate vaccine**

(A) Diagram of human ACE2 transgenic (hACE2 Tg) mouse immunization and challenge. Six- to 8-week-old hACE2 Tg mice were immunized with three doses of the candidate vaccine or placebo (control) via the intranasal route at 14-day intervals or primed via the intraperitoneal route with 100 U of inactivated SARS-CoV-2 vaccine and then boosted at 28 days with the same dose of the inactivated vaccine. Seven days after the last immunization, the mice were bled, and S-, RBD-, and N-specific IgG antibodies, S- and RBD- IgA antibodies, and NAbs in the serum were evaluated. On day 10 after the last immunization, mice were challenged intranasally with $10^3$ PFU of SARS-CoV-2. The challenged mice were monitored for mortality and weight loss for 7 days after infection.

(B–D) The antibody responses in the serum of vaccinated mice at 7 days after the last immunization were evaluated. An ELISA method was used to measure SARS-CoV-2 S-, RBD-, and N- specific IgG antibodies (B), NAbs (C), and IgA levels (D). n = 4 mice per group.

(E) Survival: placebo-immunized mice were humanely euthanized at 4 dpi (n = 4) and 5 dpi (n = 6) due to IMBCAMS-defined endpoints (n = 6–14 mice per group per time point).

(F) Weight loss (n = 6–14 mice per group per time point). Data are expressed as the mean ± the SEM. The dotted line indicates the limit of detection (LOD), and values that fell below the detection limit are represented by the limit of detection value for statistical analysis.

Significance was determined via one-way ANOVA with a Tukey multiple comparison test. *$p < 0.05$, **$p < 0.01$, ***$p < 0.001$. Asterisks in (F) indicate statistical significance compared with weight of before infection by the unpaired two-sided Student's t test (**$p < 0.01$).

Next, we assessed the histopathologic effects of the candidate vaccine on tissues. The lungs of mice treated with the placebo and challenged with SARS-CoV-2 exhibited evidence of viral pneumonia characterized by lung interstitium thickening, congested capillaries in the alveolar walls, and markedly increased macrophages at 2 dpi (Figure 6F). Mice in the placebo group at 4 dpi (n = 4) or 5 dpi (n = 6) displayed extensive capillary dilatation, congestion of the alveolar wall, and increased inflammatory cell infiltration, with most of the inflammatory cells being lymphocytes; these changes were indicative of severe disease. In contrast, both candidate vaccine-immunized mice and inactivated vaccine-immunized mice showed less evidence of viral pneumonia (Figure 6F). These findings were consistent with the absence of infectious virus in vaccinated animals. Immunohistochemical (IHC) staining evaluating the SARS-CoV-2 N protein revealed that the lungs of placebo-vaccinated mice were densely

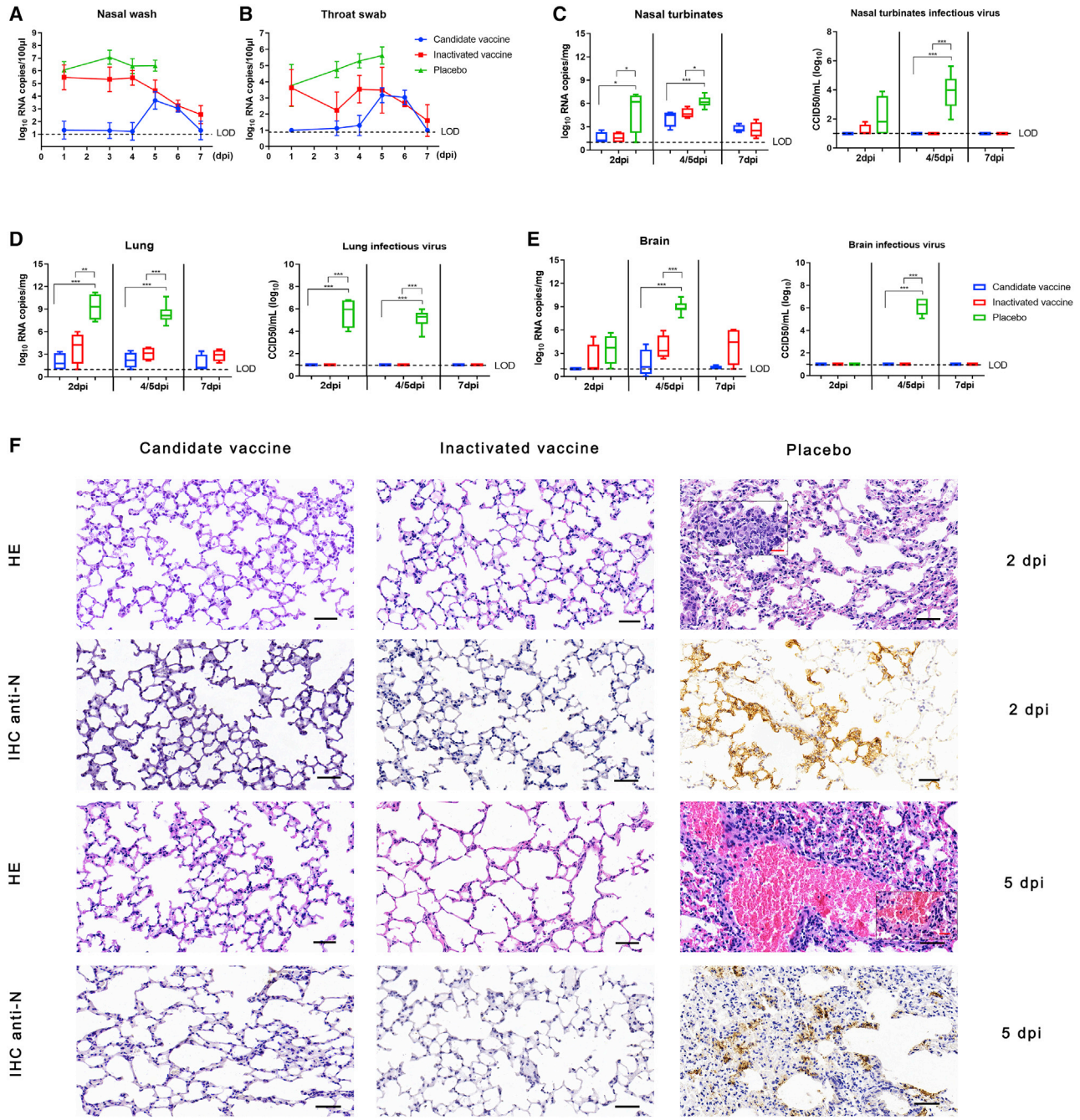


**Figure 6. Intranasal-immunized candidate vaccine offers superior protection at URT against challenge with SARS-CoV-2**

(A–D) Nasal wash (A) and throat swab (B) samples were collected for 7 days in the vaccinated groups and until animals succumbed to infection in the placebo group (by 5 dpi) (n = 4–10 mice per group per time point). RNA was extracted, and viral RNA was assessed as copies per 100 μL. Four animals were euthanized at 2, 5, and 7 dpi in the vaccinated group. For the placebo group, four animals were euthanized at 2 dpi, four animals were euthanized based on humane endpoints at 4 dpi, and six animals were humanly euthanized at 5 dpi. Tissue samples were collected, and viral RNA was assessed as copies per mg. Viral RNA and infectious virus loads in nasal turbinates (C), lungs (D), and brains were determined (n = 4–10 mice per group per time point).

(F) Images showing H&E staining and IHC staining for the SARS-CoV-2 N protein following infection with $10^3$ PFU/mouse. The images shown are from 2 and 5 dpi for all groups. Scale bar, 50 or 20 μm (insets). Each image is representative of a group of 4 mice for 2 dpi and 4 or 6 mice for 5 dpi. The dotted line indicates the limit of detection (LOD), and values below the detection limit are represented by the value of the detection limit for statistical analysis. Data are expressed as the mean ± the SEM. The dotted line indicates the limit of detection (LOD), and values that fell below the detection limit are represented by the limit of detection value for statistical analysis. Significance was determined via one-way ANOVA with a Tukey multiple comparison test. *$p < 0.05$, **$p < 0.01$, ***$p < 0.001$. See also Figure S5.

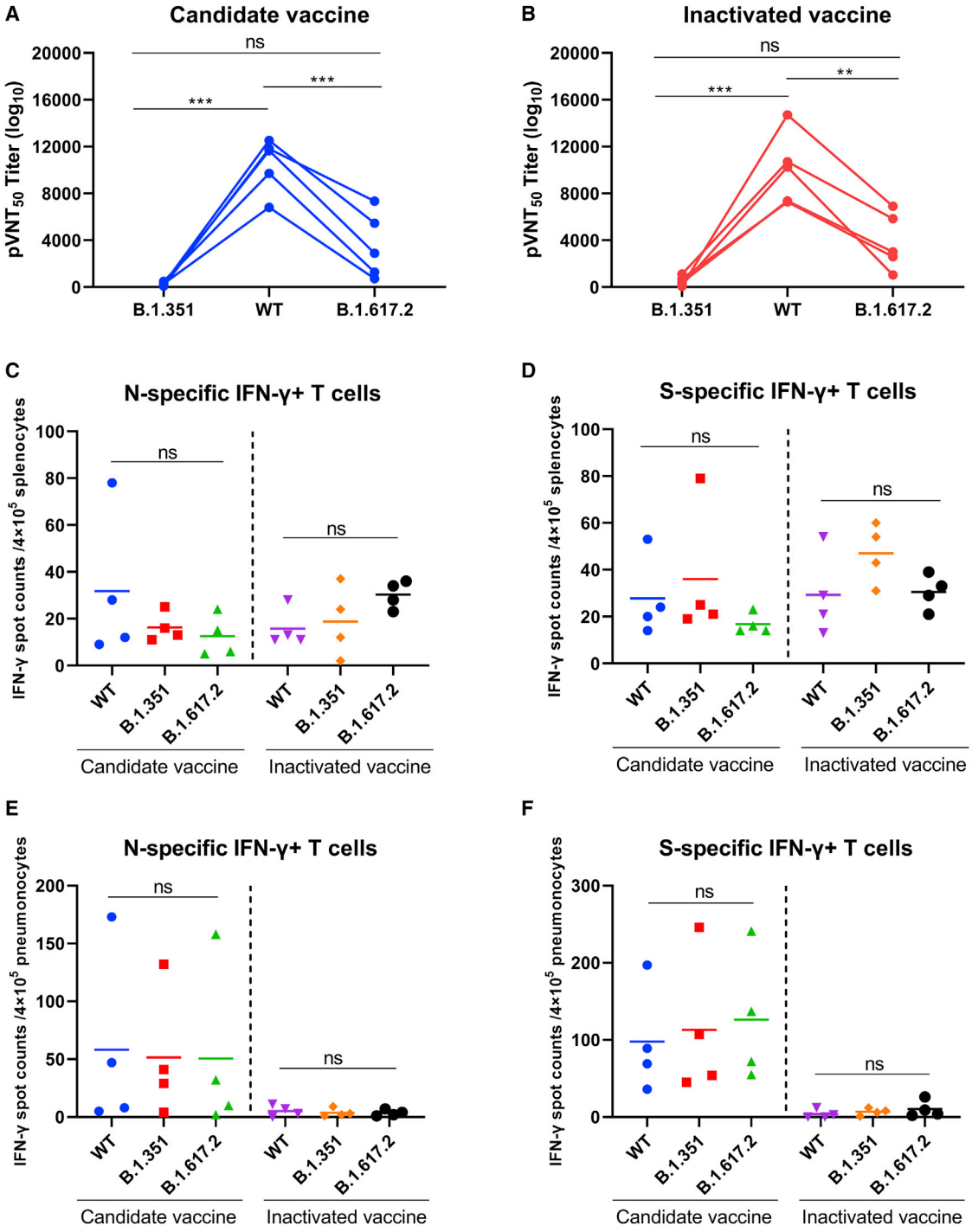


**Figure 7. Neutralization of SARS-CoV-2 pseudovirus in sera and detection of N- and S-specific T cell responses against the B.1351 and B.1.617.2 variants**

SARS-CoV-2 wild-type (WT), B.1.351 variant, or B.1.617 variant pseudoviruses were incubated with different serum sample dilutions for 1 h at 37°C before the mixtures were added to ACE2-overexpressing 293T cells. Transduction efficiency was quantified by measuring virus-encoded luciferase activity in cell lysates 48 h after transduction and used to calculate the serum dilution factor that resulted in a 50% reduction in pseudovirus particles that were associated with different degrees of S protein-mediated cell entry.

(A and B) The 50% pseudovirus neutralization ($pVNT_{50}$) in serum from mice immunized with the candidate vaccine (A) and mice immunized with the inactivated vaccine (B) against the B.1.351 and B.1.617.2 variants compared with that against the wild-type (WT) virus (n = 4 mice per group).

*(legend continued on next page)*

distributed with N-expressing cells, but this phenomenon was not seen in all the vaccine-immunized mice (Figure 6F). Collectively, these data indicated that both the candidate vaccine and the inactivated vaccine could markedly reduce lesions and SARS-CoV-2 infection in the lungs of challenged hACE2 Tg mice. In addition, we also evaluated the SARS-CoV-2 N protein in nasal tissues via IHC staining. Both placebo-immunized mice and inactivated vaccine-immunized mice showed higher levels of N-expressing cells, which was in line with the higher copy numbers of viral RNA in the NW, than candidate vaccine-immunized mice (Figure S5).

### NAbs have reduced activity against B.1.351 and B.1.617.2 variants, but specific T cell responses are still comparable

We assessed the serum levels of candidate vaccine- and inactivated vaccine-elicited NAbs against the B.1.351 and B.1.617.2 variants compared with the wild-type (WT) pseudovirus. All the serum samples efficiently inhibited entry of the WT pseudovirus. However, the neutralization ability of sera from candidate vaccine- and inactivated vaccine-immunized mice against B.1.351 was reduced by more than 39- and 20-fold compared to the neutralization ability against WT, respectively (Figures 7A and 7B). The neutralization of B.1.617.2 particles was also reduced, with a 3-fold reduction in both the candidate vaccine and inactivated vaccine groups (Figures 7A and 7B).

Next, we assessed T cell responses to both B.1.351 and B.1.617.2 using commercially available proteins that specifically included the mutated regions and compared these responses with those elicited with the corresponding vaccine control proteins. Both N- and S-specific T cell responses were detected in the splenocytes of the candidate vaccine group and the inactivated vaccine group, and in both groups no differences were observed between IFN-$\gamma$ T cell responses to the WT N/S proteins and the B.1.351 N/S proteins or between the responses to the WT N/S proteins and the B.1.617.2 N/S proteins (Figures 7C and 7D). In the lung tissues, we also did not observe any significant differences in the candidate vaccine group, but minimal T cell responses were observed in the inactivated vaccine group (Figures 7E and 7F). Together, these data indicated that the NAbs elicited by both vaccines showed greatly reduced cross-neutralization against the B.1.351 and B.1.617.2 variants compared to the homologous virus, but the T cell responses against the N and S mutations of the B.1.351 and B.1.617.2 variants were not different.

## DISCUSSION

SARS-CoV-2 exhibits more rapid transmission than other coronaviruses (Chan et al., 2020), and more transmissible variants with the potential of breakthrough infections are emerging, leading to the urgent need for a prophylactic vaccine to prevent disease and infection and confer broad immunity toward drift variants. To date, several vaccines, such as mRNA vaccines, adenoviral vector vaccines, and inactivated vaccines, have been authorized for emergency use based on their good induction of humoral and/or cellular immunity; however, the mucosal humoral immunity and robust local T cell responses needed for viral clearance in the URT have not been exhibited (Corbett et al., 2020; Gao et al., 2020; van Doremalen et al., 2020). Therefore, mucosal vaccines are an ideal strategy for clearing the input nasal virus and preventing virus transmission. Here, based on the concept that combined activation of multiple PRRs (pattern recognition receptors) can exert synergistic effects and induce strong adaptive immune responses (Kasturi et al., 2011; Mount et al., 2013; Trinchieri and Sher, 2007; Yildiz et al., 2015), we combined two classes of adjuvants, KF and cGAMP, that activate the TLR-dependent and TLR-independent DNA recognition pathways, respectively; we attempted to employ a combined adjuvant approach to develop an improved mucosal adjuvant. We showed that intranasal administration of a candidate vaccine comprising the N protein and $SFL_{mut}$ protein supplemented with this rationally designed combined adjuvant could induce high levels of functional immunity in mice, protect mice expressing hACE2 from lethal SARS-CoV-2 challenge, and result in more effective viral clearance from the URT compared with an inactivated vaccine.

Full-length S-protein and fragments of S-protein, such as S1 or RBD have been shown a great potential to be effective vaccine candidates against SARS-CoV-2 in many studies (Jangra et al., 2021; Routhu et al., 2021). However, in the current study, we further demonstrated that the effective immunity induced by the candidate vaccine is dependent on antigen components, especially depending on the state of the S protein. In the serum, although all the experimental vaccines containing different S proteins including RBD, S1, SFL, or $SFL_{mut}$ could induce antibodies against the S protein and RBD, NAbs against SARS-CoV-2 were induced only in the mice in the $SFL_{mut}$ group. In the NW and BALF, IgA antibodies against the S protein and RBD were induced, with higher antibody levels in the $SFL_{mut}$ group than in all the other groups. Indeed, a study on rhesus macaques evaluated DNA vaccine protection against SARS-CoV-2 and found that the protection elicited with the full-length S protein was better than that achieved with smaller fragments (S1 and the RBD) (Yu et al., 2020). Additionally, several studies have indicated that nonmutated SFL does not induce ideal humoral and mucosal immune responses, which may be due to the "down" state being the predominant state of nonmutated SFL and therefore limiting the RBD-directed response (Cai et al., 2020; Fan et al., 2020; Turoňová et al., 2020). Thus, researchers generated the $SFL_{mut}$ protein from the full-length S protein with several amino acid mutations to confer protease resistance, stabilize the construct in a prefusion conformation, and increase immunogenicity, thermostability, and protein yield

(C–F) Antigen-specific activation of T cells by the N and S proteins of the B.1.351 and B.1.617.2 variants compared with the homologous WT proteins. N-specific (C) and S-specific (D) activation of T cells in splenocytes from mice immunized with the candidate vaccine or the inactivated vaccine at 14 days after the third immunization. N-specific (E) and S-specific (F) activation of T cells in lung tissues from mice immunized with the candidate vaccine or the inactivated vaccine at 14 days after the third immunization (n = 4 mice per group). Significance was determined via one-way ANOVA with a Tukey multiple comparison test. *$p < 0.05$, **$p < 0.01$, ***$p < 0.001$, ns, no significance.

(Hsieh et al., 2020; Wrapp et al., 2020). For example, the Novavax vaccine NVX-CoV2373 is generated with 682-QQAQ-685 mutations and two proline substitutions (K986P and V987P), which have achieved good efficacy in a clinical trial (Bangaru et al., 2020; Keech et al., 2020). In comparison, the $SFL_{mut}$ protein used in this study was generated with eight mutations (R683A, R685A, F817P, A892P, A899P, A942P, K986P, and V987P), which mainly increase thermostability and protein yield and may strengthen immunogenicity (Hsieh et al., 2020).

Except NAbs, there is growing evidence that IgA plays an important role in natural and optimal vaccine-induced immunity to SARS-CoV-2 (Fourati et al., 2020; Sterlin et al., 2021; Zeng et al., 2021). Sterlin et al. (2021) has shown that serum IgA is a potent and early SARS-CoV-2-neutralizing antibody that dominates early SARS-CoV-2-specific humoral responses. Encouragingly, the titer of IgA in the NW has been demonstrated to limit virus transmission and reduce the risk of hospitalization in SARS-CoV-2-infected individuals (Butler et al., 2021; Sterlin et al., 2021). In our study, we found that N and $SFL_{mut}$ proteins formulated with the combined adjuvant and administered via the i.n. route could elicit robust S- and RBD-specific IgA responses and weak N-specific IgA responses in the respiratory tract. Furthermore, significant local $IgA^+$ B cell responses were observed in the NALT of mice immunized with the candidate vaccine after the last immunization. The RNA-seq results also indicated that the levels of many genes associated with B cell proliferation were increased in the NALT. Previous studies have demonstrated that upon intranasal antigen exposure, the major antibody isotype produced by B cells in the NALT is IgA (Heritage et al., 1997; Wu et al., 1996). Research on influenza confirmed that IgA molecules in NW can directly mediate local anti-influenza immunity, which indicated the importance of IgA in protection against virus infection in URT (Renegar and Small, 1991). Since mucosal IgA plays a crucial role in the immune defense of mucosal surfaces, which are the first point of entry of respiratory pathogens, by neutralizing viruses or impeding their attachment to epithelial cells, we inferred that robust IgA production elicited by the candidate vaccine played a significant role in the rapid viral clearance of the URT.

Although IgA plays a crucial role in mucosal immunity against viruses, T lymphocytes and some immune factors, such as cytokines in the respiratory tract, also play an irreplaceable role in the immune defense of mucosa and virus clearance. Candidate vaccine intranasal-immunized mice showed significant local $CD8^+$ T cell responses in the NALT after the last immunization, which was also demonstrated by the transcriptomic profiling of several chemokines involved in T cell activation. For example, the expression of the Spp1 and CCL19 genes, which are involved in the recruitment and induction of T cells and the generation of memory $CD8^+$ T cells (Mazzali et al., 2002; Morimoto et al., 2011; Yan et al., 2019), was markedly increased in the NALT in mice immunized with the candidate vaccine. Moreover, mice immunized with the candidate vaccine showed high levels of $CD4^+$ TRM cells and $CD8^+$ TRM cells, which play important roles in viral clearance (Rosato et al., 2017; Turner et al., 2014). Notably, an important cell chemotaxis molecule, CD74, was highly expressed in the nasal mucosa of mice immunized with the candidate vaccine. There is ample evidence showing that CD74 can significantly regulate T and B cell development, DC motility, and thymic selection (Leth-Larsen et al., 2009) and is beneficial to mucosal immune responses. A recent study indicated that CD74 is involved in blocking the cathepsin-mediated cleavage of SARS-CoV-2 glycoproteins, thereby preventing viral fusion (Bruchez et al., 2020). Additionally, we found enhanced expression of genes in response to IFN-$\beta$ and IFN-$\gamma$ in the mucosa of the candidate vaccine group. Evidence shows that interferon levels, including type I and type II interferon levels, increased after CoVs infection, which could induce a host defense mechanism against virus because of its strong capacity to inhibit the replication of CoVs (Hoagland et al., 2021; Kindler et al., 2016; Singh et al., 2021).

The emergence of SARS-CoV-2 variants, especially B.1.351 in South Africa and B.1.617.2 in India, has caused great concern that these variants may evade the NAbs produced in response to infection or vaccination (Arora et al., 2021; Wang et al., 2021a). In the current study, we evaluated the ability of the candidate vaccine to cross-neutralize the B.1.351 and B.1.617.2 variants, and the results were consistent with recent research of lower levels of NAbs against B.1.351 and B.1.617.2 variants (Wall et al., 2021). In addition, we performed an ELISpot assay of N- and S-specific T cell responses from mice immunized with the candidate vaccine and inactivated vaccine. We found that T cell activation in splenocytes induced by both the candidate vaccine and inactivated vaccine showed no significant difference against the homologous virus and the B.1.351 and B.1.617.2 variants. T cell activation in lung tissues was also observed in mice immunized with the candidate vaccine and showed no significant difference in response to the B.1.351 and B.1.617.2 variants compared with the response to the homologous virus. However, we did not find an obvious T cell response to any of the strains in the lung tissues of mice immunized with the inactivated vaccine. A recent study by Geers et al. (2021) also demonstrated that SARS-CoV-2 variants may partially escape humoral immune responses but not T cell responses. Studies on influenza virus infection suggest that respiratory T cells elicit cross-protection against influenza virus variants (van de Ven et al., 2020). Thus, we deduced that cross T cell responses, especially the local T cell responses, induced by candidate vaccines might protect against SARS-CoV-2 variants infection to some extent, although further *in vivo* challenge studies are required in the future.

In conclusion, the candidate vaccine containing the SARS-CoV-2 $SFL_{mut}$ and N proteins with a combination of the adjuvants KF and cGAMP elicited strong systemic and mucosal immune responses and protected hACE2 Tg mice from lethal SARS-CoV-2 challenge. The robust viral clearance in the URT induced via intranasal immunization with the candidate vaccine might make this vaccine an ideal vaccine for protection against both disease and infection. Further evaluation in nonhuman primates and clinical trials should be performed. We also identified a mucosal adjuvant combination comprising an agonist of STING and a ligand for TLR5, which can be further developed for use as a combination mucosal adjuvant for other coronaviruses and respiratory viruses.

### Limitations of this study

In this study, the developed mucosal vaccine, comprising N and $SFL_{mut}$ protein adjuvanted with KF and cGAMP, showed robust viral clearance in the URT, which might make it a potential vaccine for preventing infection and transmission of SARS-CoV-2. We acknowledge that the efficacy of preventing transmission will required to be explored further with the more extensive animal models, such as hamsters and non-human primates. Moreover, while we interpreted that the IgA antibodies, T lymphocytes, and some immune factors eliciting by candidate vaccine may contribute to robust viral clearance in the respiratory tract, we don't know in what extent these immune responses directly contribute to vaccine efficacy. The specific protective mechanisms of those effects inducing by candidate vaccine still need more studies. In addition, although we observed cross-reactive T cell responses against B.1.351 and B.1.617.2 variants *in vitro*, whether cross-protection eliciting by a candidate vaccine exists needs to be determined with more *in vivo* studies.

## STAR★METHODS

Detailed methods are provided in the online version of this paper and include the following:

- KEY RESOURCES TABLE
- RESOURCE AVAILABILITY
  - Lead contact
  - Materials availability
  - Data and code availability
- EXPERIMENTAL MODEL AND SUBJECT DETAILS
  - Viruses and cells
  - Mice and ethics statements
- METHOD DETAILS
  - Isolation and stimulation of dendritic cells
  - Vaccine formulations
  - Mouse experiments
  - Enzyme linked immunosorbent assay
  - SARS-CoV-2 neutralization assay
  - Enzyme-linked immunospot assay
  - Detection of lung tissue-resident cells
  - Flow cytometry
  - RNA-seq
  - Measurement of viral burden
  - Virus titration
  - Histopathology and immunohistochemistry
  - Pseudovirus neutralization assay
- QUANTIFICATION AND STATISTICAL ANALYSIS

### SUPPLEMENTAL INFORMATION

Supplemental information can be found online at https://doi.org/10.1016/j.celrep.2021.110112.

### ACKNOWLEDGMENTS

This work was financially supported by the Yunnan Provincial Science and Technology Department (grant 2019HC006) and the Kunming Science and Technology Department (grant 2020-1-N-037). We sincerely thank Dr. Yan Huimin and Jingyi Yang (Wuhan Institute of Virology, Chinese Academy of Sciences) for providing the non-pathogenic *E. coli*-derived flagellin (KF) plasmid and assisting with the KF purification and the Professor WeiJin Huang from the Institute for Biological Product Control, National Institutes for Food and Drug Control, Beijing, China, for assisting with ACE2-overexpressed 293T cells (293T-ACE2).

### AUTHOR CONTRIBUTIONS

Conceptualization and methodology, L.S., M.B.S., and L.D.L.; investigation, W.W.J., L.K.C., X.Y.W., J.Y.L., H.L., J.L.L., J.L., and G.J.; resources, J.L. and L.D.L.; data curation, W.W.J., X.Y.W., and L.K.C.; writing – original draft, W.W.J., L.S., and L.K.C.; writing – review and editing, M.B.S. and L.D.L.; supervision, J.L.L., G.J., H.L., and Q.G.; funding acquisition, M.B.S.

### DECLARATION OF INTERESTS

The authors declare no competing interests.

Received: June 8, 2021
Revised: November 6, 2021
Accepted: November 18, 2021
Published: November 24, 2021

### REFERENCES

Anderson, K.G., Mayer-Barber, K., Sung, H., Beura, L., James, B.R., Taylor, J.J., Qunaj, L., Griffith, T.S., Vezys, V., Barber, D.L., and Masopust, D. (2014). Intravascular staining for discrimination of vascular and tissue leukocytes. Nat. Protoc. *9*, 209–222.

Arora, P., Sidarovich, A., Krüger, N., Kempf, A., Nehlmeier, I., Graichen, L., Moldenhauer, A.S., Winkler, M.S., Schulz, S., Jäck, H.M., et al. (2021). B.1.617.2 enters and fuses lung cells with increased efficiency and evades antibodies induced by infection and vaccination. Cell Rep. *37*, 109825.

Bangaru, S., Ozorowski, G., Turner, H.L., Antanasijevic, A., Huang, D., Wang, X., Torres, J.L., Diedrich, J.K., Tian, J.H., Portnoff, A.D., et al. (2020). Structural analysis of full-length SARS-CoV-2 spike protein from an advanced vaccine candidate. Science *370*, 1089–1094.

Barnes, C.O., West, A.P., Jr., Huey-Tubman, K.E., Hoffmann, M.A.G., Sharaf, N.G., Hoffman, P.R., Koranda, N., Gristick, H.B., Gaebler, C., Muecksch, F., et al. (2020). Structures of human antibodies bound to SARS-CoV-2 spike reveal common epitopes and recurrent features of antibodies. Cell *182*, 828–842.

Bian, L., Gao, F., Zhang, J., He, Q., Mao, Q., Xu, M., and Liang, Z. (2021). Effects of SARS-CoV-2 variants on vaccine efficacy and response strategies. Expert Rev. Vaccines *20*, 365–373.

Blaauboer, S.M., Mansouri, S., Tucker, H.R., Wang, H.L., Gabrielle, V.D., and Jin, L. (2015). The mucosal adjuvant cyclic di-GMP enhances antigen uptake and selectively activates pinocytosis-efficient cells in vivo. eLife *4*, e06670.

Bruchez, A., Sha, K., Johnson, J., Chen, L., Stefani, C., McConnell, H., Gaucherand, L., Prins, R., Matreyek, K.A., Hume, A.J., et al. (2020). MHC class II transactivator CIITA induces cell resistance to Ebola virus and SARS-like coronaviruses. Science *370*, 241–247.

Burdette, D.L., and Vance, R.E. (2013). STING and the innate immune response to nucleic acids in the cytosol. Nat. Immunol. *14*, 19–26.

Burdette, D.L., Monroe, K.M., Sotelo-Troha, K., Iwig, J.S., Eckert, B., Hyodo, M., Hayakawa, Y., and Vance, R.E. (2011). STING is a direct innate immune sensor of cyclic di-GMP. Nature *478*, 515–518.

Butler, S.E., Crowley, A.R., Natarajan, H., Xu, S., Weiner, J.A., Bobak, C.A., Mattox, D.E., Lee, J., Wieland-Alter, W., Connor, R.I., et al. (2021). Distinct features and functions of systemic and mucosal humoral immunity among SARS-CoV-2 convalescent individuals. Front. Immunol. *11*, 618685.

Cai, Y., Zhang, J., Xiao, T., Peng, H., Sterling, S.M., Walsh, R.M., Jr., Rawson, S., Rits-Volloch, S., and Chen, B. (2020). Distinct conformational states of SARS-CoV-2 spike protein. Science *369*, 1586–1592.

Chan, J.F.W., Yuan, S., Kok, K.H., To, K.K.W., Chu, H., Yang, J., Xing, F., Liu, J., Yip, C.C.Y., Poon, R.W.S., et al. (2020). A familial cluster of pneumonia associated with the 2019 novel coronavirus indicating person-to-person transmission: a study of a family cluster. Lancet *395*, 514–523.

Che, Y., Liu, X., Pu, Y., Zhou, M., Zhao, Z., Jiang, R., Yin, Z., Xu, M., Yin, Q., Wang, J., et al. (2020). Randomized, double-blinded and placebo-controlled phase II trial of an inactivated SARS-CoV-2 vaccine in healthy adults. Clin. Infect. Dis., ciaa1703.

Cock, P.J., Fields, C.J., Goto, N., Heuer, M.L., and Rice, P.M. (2010). The Sanger FASTQ file format for sequences with quality scores, and the Solexa/Illumina FASTQ variants. Nucleic Acids Res. *38*, 1767–1771.

Corbett, K.S., Flynn, B., Foulds, K.E., Francica, J.R., Boyoglu-Barnum, S., Werner, A.P., Flach, B., O'Connell, S., Bock, K.W., Minai, M., et al. (2020). Evaluation of the mRNA-1273 vaccine against SARS-CoV-2 in nonhuman primates. N. Engl. J. Med. *383*, 1544–1555.

Dangi, T., Class, J., Palacio, N., Richner, J.M., and Penaloza MacMaster, P. (2021). Combining spike- and nucleocapsid-based vaccines improves distal control of SARS-CoV-2. Cell Rep. *36*, 109664.

Dutta, N.K., Mazumdar, K., and Gordy, J.T. (2020). The nucleocapsid protein of SARS-CoV-2: a target for vaccine development. J. Virol. *94*, e00647, e20.

Fan, X., Cao, D., Kong, L., and Zhang, X. (2020). Cryo-EM analysis of the post-fusion structure of the SARS-CoV spike glycoprotein. Nat. Commun. *11*, 3618.

Ferretti, A.P., Kula, T., Wang, Y., Nguyen, D.M.V., Weinheimer, A., Dunlap, G.S., Xu, Q., Nabilsi, N., Perullo, C.R., Cristofaro, A.W., et al. (2020). Unbiased screens show CD8(+) T cells of COVID-19 patients recognize shared epitopes in SARS-CoV-2 that largely reside outside the spike protein. Immunity *53*, 1095–1107.

Flores-Langarica, A., Marshall, J.L., Hitchcock, J., Cook, C., Jobanputra, J., Bobat, S., Ross, E.A., Coughlan, R.E., Henderson, I.R., Uematsu, S., et al. (2012). Systemic flagellin immunization stimulates mucosal CD103+ dendritic cells and drives Foxp3+ regulatory T cell and IgA responses in the mesenteric lymph node. J. Immunol. *189*, 5745–5754.

Fourati, S., Hue, S., Pawlotsky, J.M., Mekontso-Dessap, A., and de Prost, N. (2020). SARS-CoV-2 viral loads and serum IgA/IgG immune responses in critically ill COVID-19 patients. Intensive Care Med. *46*, 1781–1783.

Gao, Q., Bao, L., Mao, H., Wang, L., Xu, K., Yang, M., Li, Y., Zhu, L., Wang, N., Lv, Z., et al. (2020). Development of an inactivated vaccine candidate for SARS-CoV-2. Science *369*, 77–81.

Geers, D., Shamier, M.C., Bogers, S., den Hartog, G., Gommers, L., Nieuwkoop, N.N., Schmitz, K.S., Rijsbergen, L.C., van Osch, J.A.T., Dijkhuizen, E., et al. (2021). SARS-CoV-2 variants of concern partially escape humoral but not T-cell responses in COVID-19 convalescent donors and vaccinees. Sci. Immunol. *6*, eabj1750.

He, J., Huang, J.R., Zhang, Y.L., and Zhang, J. (2021). SARS-CoV-2 nucleocapsid protein intranasal inoculation induces local and systemic T cell responses in mice. J. Med. Virol. *93*, 1923–1925.

Henderson, R., Edwards, R.J., Mansouri, K., Janowska, K., Stalls, V., Gobeil, S.M.C., Kopp, M., Li, D., Parks, R., Hsu, A.L., et al. (2020). Controlling the SARS-CoV-2 spike glycoprotein conformation. Nat. Struct. Mol. Biol. *27*, 925–933.

Heritage, P.L., Underdown, B.J., Arsenault, A.L., Snider, D.P., and McDermott, M.R. (1997). Comparison of murine nasal-associated lymphoid tissue and Peyer's patches. Am. J. Respir. Crit. Care Med. *156*, 1256–1262.

Hoagland, D.A., Møller, R., Uhl, S.A., Oishi, K., Frere, J., Golynker, I., Horiuchi, S., Panis, M., Blanco-Melo, D., Sachs, D., et al. (2021). Leveraging the antiviral type I interferon system as a first line of defense against SARS-CoV-2 pathogenicity. Immunity *54*, 557–570.

Honko, A.N., and Mizel, S.B. (2005). Effects of flagellin on innate and adaptive immunity. Immunol. Res. *33*, 83–101.

Hsieh, C.L., Goldsmith, J.A., Schaub, J.M., DiVenere, A.M., Kuo, H.C., Javanmardi, K., Le, K.C., Wrapp, D., Lee, A.G., Liu, Y., et al. (2020). Structure-based design of prefusion-stabilized SARS-CoV-2 spikes. Science *369*, 1501–1505.

Huang, Y., Yang, C., Xu, X.F., Xu, W., and Liu, S.W. (2020). Structural and functional properties of SARS-CoV-2 spike protein: potential antivirus drug development for COVID-19. Acta Pharmacol. Sin. *41*, 1141–1149.

Jangra, S., Landers, J.J., Rathnasinghe, R., O'Konek, J.J., Janczak, K.W., Cascalho, M., Kennedy, A.A., Tai, A.W., Baker, J.R., Jr., Schotsaert, M., and Wong, P.T. (2021). A Combination Adjuvant for the Induction of Potent Antiviral Immune Responses for a Recombinant SARS-CoV-2 Protein Vaccine. Front. Immunol. *12*, 729189.

Karaolis, D.K.R., Newstead, M.W., Zeng, X., Hyodo, M., Hayakawa, Y., Bhan, U., Liang, H., and Standiford, T.J. (2007). Cyclic di-GMP stimulates protective innate immunity in bacterial pneumonia. Infect. Immun. *75*, 4942–4950.

Karim, S.S.A. (2021). Vaccines and SARS-CoV-2 variants: the urgent need for a correlate of protection. Lancet *397*, 1263–1264.

Kasturi, S.P., Skountzou, I., Albrecht, R.A., Koutsonanos, D., Hua, T., Nakaya, H.I., Ravindran, R., Stewart, S., Alam, M., Kwissa, M., et al. (2011). Programming the magnitude and persistence of antibody responses with innate immunity. Nature *470*, 543–547.

Keech, C., Albert, G., Cho, I., Robertson, A., Reed, P., Neal, S., Plested, J.S., Zhu, M., Cloney-Clark, S., Zhou, H., et al. (2020). Phase 1–2 trial of a SARS-CoV-2 recombinant spike protein nanoparticle vaccine. N. Engl. J. Med. *383*, 2320–2332.

Kim, D., Langmead, B., and Salzberg, S.L. (2015). HISAT: a fast spliced aligner with low memory requirements. Nat. Methods *12*, 357–360.

Kindler, E., Thiel, V., and Weber, F. (2016). Interaction of SARS and MERS Coronaviruses with the Antiviral Interferon Response. Adv. Virus Res. *96*, 219–243.

Krammer, F. (2020). SARS-CoV-2 vaccines in development. Nature *586*, 516–527.

Leth-Larsen, R., Lund, R., Hansen, H.V., Laenkholm, A.V., Tarin, D., Jensen, O.N., and Ditzel, H.J. (2009). Metastasis-related plasma membrane proteins of human breast cancer cells identified by comparative quantitative mass spectrometry. Mol. Cell. Proteomics *8*, 1436–1449.

Letko, M., Marzi, A., and Munster, V. (2020). Functional assessment of cell entry and receptor usage for SARS-CoV-2 and other lineage B betacoronaviruses. Nat. Microbiol. *5*, 562–569.

Love, M.I., Huber, W., and Anders, S. (2014). Moderated estimation of fold change and dispersion for RNA-seq data with DESeq2. Genome Biol. *15*, 550.

Luo, J., Liu, X.P., Xiong, F.F., Gao, F.X., Yi, Y.L., Zhang, M., Chen, Z., and Tan, W.S. (2019). Enhancing immune response and heterosubtypic protection ability of inactivated H7N9 vaccine by using STING agonist as a mucosal adjuvant. Front. Immunol. *10*, 2274.

Lurie, N., Saville, M., Hatchett, R., and Halton, J. (2020). Developing covid-19 vaccines at pandemic speed. N. Engl. J. Med. *382*, 1969–1973.

Martin, T.L., Jee, J., Kim, E., Steiner, H.E., Cormet-Boyaka, E., and Boyaka, P.N. (2017). Sublingual targeting of STING with 3'3'-cGAMP promotes systemic and mucosal immunity against anthrax toxins. Vaccine *35*, 2511–2519.

Mazzali, M., Kipari, T., Ophascharoensuk, V., Wesson, J.A., Johnson, R., and Hughes, J. (2002). Osteopontin–a molecule for all seasons. QJM *95*, 3–13.

Mizel, S.B., and Bates, J.T. (2010). Flagellin as an adjuvant: cellular mechanisms and potential. J. Immunol. *185*, 5677–5682.

Morimoto, J., Sato, K., Nakayama, Y., Kimura, C., Kajino, K., Matsui, Y., Miyazaki, T., and Uede, T. (2011). Osteopontin modulates the generation of memory CD8+ T cells during influenza virus infection. J. Immunol. *187*, 5671–5683.

Mount, A., Koernig, S., Silva, A., Drane, D., Maraskovsky, E., and Morelli, A.B. (2013). Combination of adjuvants: the future of vaccine design. Expert Rev. Vaccines *12*, 733–746.

Ni, L., Ye, F., Cheng, M.L., Feng, Y., Deng, Y.Q., Zhao, H., Wei, P., Ge, J., Gou, M., Li, X., et al. (2020). Detection of SARS-CoV-2-specific humoral and cellular immunity in COVID-19 convalescent individuals. Immunity *52*, 971–977.

Oliveira, S.C., de Magalhães, M.T.Q., and Homan, E.J. (2020). Immunoinformatic analysis of SARS-CoV-2 nucleocapsid protein and identification of COVID-19 vaccine targets. Front. Immunol. *11*, 587615.

Polack, F.P., Thomas, S.J., Kitchin, N., Absalon, J., Gurtman, A., Lockhart, S., Perez, J.L., Pérez Marc, G., Moreira, E.D., Zerbini, C., et al.; C4591001 Clinical Trial Group (2020). Safety and efficacy of the BNT162b2 mRNA covid-19 vaccine. N. Engl. J. Med. *383*, 2603–2615.

Prévost, J., and Finzi, A. (2021). The great escape? SARS-CoV-2 variants evading neutralizing responses. Cell Host Microbe *29*, 322–324.

Ramasamy, M.N., Minassian, A.M., Ewer, K.J., Flaxman, A.L., Folegatti, P.M., Owens, D.R., Voysey, M., Aley, P.K., Angus, B., Babbage, G., et al.; Oxford COVID Vaccine Trial Group (2021). Safety and immunogenicity of ChAdOx1 nCoV-19 vaccine administered in a prime-boost regimen in young and old adults (COV002): a single-blind, randomised, controlled, phase 2/3 trial. Lancet *396*, 1979–1993.

Renegar, K.B., and Small, P.A., Jr. (1991). Immunoglobulin A mediation of murine nasal anti-influenza virus immunity. J. Virol. *65*, 2146–2148.

Rosato, P.C., Beura, L.K., and Masopust, D. (2017). Tissue resident memory T cells and viral immunity. Curr. Opin. Virol. *22*, 44–50.

Routhu, N.K., Cheedarla, N., Bollimpelli, V.S., Gangadhara, S., Edara, V.V., Lai, L., Sahoo, A., Shiferaw, A., Styles, T.M., Floyd, K., et al. (2021). SARS-CoV-2 RBD trimer protein adjuvanted with Alum-3M-052 protects from SARS-CoV-2 infection and immune pathology in the lung. Nat. Commun. *12*, 3587.

Secchi, M., Bazzigaluppi, E., Brigatti, C., Marzinotto, I., Tresoldi, C., Rovere-Querini, P., Poli, A., Castagna, A., Scarlatti, G., Zangrillo, A., et al. (2020). COVID-19 survival associates with the immunoglobulin response to the SARS-CoV-2 spike receptor binding domain. J. Clin. Invest. *130*, 6366–6378.

Singh, D.K., Singh, B., Ganatra, S.R., Gazi, M., Cole, J., Thippeshappa, R., Alfson, K.J., Clemmons, E., Gonzalez, O., Escobedo, R., et al. (2021). Responses to acute infection with SARS-CoV-2 in the lungs of rhesus macaques, baboons and marmosets. Nat. Microbiol. *6*, 73–86.

Sterlin, D., Mathian, A., Miyara, M., Mohr, A., Anna, F., Claër, L., Quentric, P., Fadlallah, J., Devilliers, H., Ghillani, P., et al. (2021). IgA dominates the early neutralizing antibody response to SARS-CoV-2. Sci. Transl. Med. *13*, eabd2223.

Sun, Y., Shi, W., Yang, J.Y., Zhou, D.H., Chen, Y.Q., Zhang, Y., Yang, Y., He, B.X., Zhong, M.H., Li, Y.M., et al. (2012). Flagellin-PAc fusion protein is a high-efficacy anti-caries mucosal vaccine. J. Dent. Res. *91*, 941–947.

Temizoz, B., Kuroda, E., and Ishii, K.J. (2018). Combination and inducible adjuvants targeting nucleic acid sensors. Curr. Opin. Pharmacol. *41*, 104–113.

Trinchieri, G., and Sher, A. (2007). Cooperation of Toll-like receptor signals in innate immune defence. Nat. Rev. Immunol. *7*, 179–190.

Turner, D.L., Bickham, K.L., Thome, J.J., Kim, C.Y., D'Ovidio, F., Wherry, E.J., and Farber, D.L. (2014). Lung niches for the generation and maintenance of tissue-resident memory T cells. Mucosal Immunol. *7*, 501–510.

Turoňová, B., Sikora, M., Schürmann, C., Hagen, W.J.H., Welsch, S., Blanc, F.E.C., von Bülow, S., Gecht, M., Bagola, K., Hörner, C., et al. (2020). In situ structural analysis of SARS-CoV-2 spike reveals flexibility mediated by three hinges. Science *370*, 203–208.

van de Ven, K., de Heij, F., van Dijken, H., Ferreira, J.A., and de Jonge, J. (2020). Systemic and respiratory T-cells induced by seasonal H1N1 influenza protect against pandemic H2N2 in ferrets. Commun. Biol. *3*, 564.

van Doremalen, N., Lambe, T., Spencer, A., Belij-Rammerstorfer, S., Purushotham, J.N., Port, J.R., Avanzato, V.A., Bushmaker, T., Flaxman, A., Ulaszewska, M., et al. (2020). ChAdOx1 nCoV-19 vaccine prevents SARS-CoV-2 pneumonia in rhesus macaques. Nature *586*, 578–582.

Wall, E.C., Wu, M., Harvey, R., Kelly, G., Warchal, S., Sawyer, C., Daniels, R., Hobson, P., Hatipoglu, E., Ngai, Y., et al. (2021). Neutralising antibody activity against SARS-CoV-2 VOCs B.1.617.2 and B.1.351 by BNT162b2 vaccination. Lancet *397*, 2331–2333.

Walls, A.C., Park, Y.J., Tortorici, M.A., Wall, A., McGuire, A.T., and Veesler, D. (2020). Structure, function, and antigenicity of the SARS-CoV-2 spike glycoprotein. Cell *181*, 281–292.

Wang, G.L., Wang, Z.Y., Duan, L.J., Meng, Q.C., Jiang, M.D., Cao, J., Yao, L., Zhu, K.L., Cao, W.C., and Ma, M.J. (2021a). Susceptibility of Circulating SARS-CoV-2 Variants to Neutralization. N. Engl. J. Med. *384*, 2354–2356.

Wang, Z., Schmidt, F., Weisblum, Y., Muecksch, F., Barnes, C.O., Finkin, S., Schaefer-Babajew, D., Cipolla, M., Gaebler, C., Lieberman, J.A., et al. (2021b). mRNA vaccine-elicited antibodies to SARS-CoV-2 and circulating variants. Nature *592*, 616–622.

Wrapp, D., Wang, N., Corbett, K.S., Goldsmith, J.A., Hsieh, C.L., Abiona, O., Graham, B.S., and McLellan, J.S. (2020). Cryo-EM structure of the 2019-nCoV spike in the prefusion conformation. Science *367*, 1260–1263.

Wu, H.Y., Nikolova, E.B., Beagley, K.W., and Russell, M.W. (1996). Induction of antibody-secreting cells and T-helper and memory cells in murine nasal lymphoid tissue. Immunology *88*, 493–500.

Yan, Y., Chen, R., Wang, X., Hu, K., Huang, L., Lu, M., and Hu, Q. (2019). CCL19 and CCR7 expression, signaling pathways, and adjuvant functions in viral infection and prevention. Front. Cell Dev. Biol. *7*, 212.

Yang, J., Wang, W., Chen, Z., Lu, S., Yang, F., Bi, Z., Bao, L., Mo, F., Li, X., Huang, Y., et al. (2020). A vaccine targeting the RBD of the S protein of SARS-CoV-2 induces protective immunity. Nature *586*, 572–577.

Yildiz, S., Alpdundar, E., Gungor, B., Kahraman, T., Bayyurt, B., Gursel, I., and Gursel, M. (2015). Enhanced immunostimulatory activity of cyclic dinucleotides on mouse cells when complexed with a cell-penetrating peptide or combined with CpG. Eur. J. Immunol. *45*, 1170–1179.

Yu, J., Tostanoski, L.H., Peter, L., Mercado, N.B., McMahan, K., Mahrokhian, S.H., Nkolola, J.P., Liu, J., Li, Z., Chandrashekar, A., et al. (2020). DNA vaccine protection against SARS-CoV-2 in rhesus macaques. Science *369*, 806–811.

Zeng, W., Ma, H., Ding, C., Yang, Y., Sun, Y., Huang, X., He, W., Xiang, Y., Gao, Y., and Jin, T. (2021). Characterization of SARS-CoV-2-specific antibodies in COVID-19 patients reveals highly potent neutralizing IgA. Signal Transduct. Target. Ther. *6*, 35.

Zhou, Y., Zhou, B., Pache, L., Chang, M., Khodabakhshi, A.H., Tanaseichuk, O., Benner, C., and Chanda, S.K. (2019a). Metascape provides a biologist-oriented resource for the analysis of systems-level datasets. Nat. Commun. *10*, 1523.

## STAR★METHODS

### KEY RESOURCES TABLE

| Reagent or resource | Source | Identifier |
|---|---|---|
| **Antibodies** | | |
| CD11c-BV510 | Biolegend | Cat# 117338; RRID: AB_2562016 |
| CD80-BV605 | Biolegend | Cat# 104729; RRID: AB_11126141 |
| CD86-PE-Cy7 | Invitrogen | Cat# 25-0862-82; RRID: AB_2573371 |
| CD40-BV421 | BD Bioscience | Cat# 562846; RRID: AB_2734767 |
| MHC Class II (I-A/I-E)-PE | Invitrogen | Cat# 12-5321-82; AB_465928 |
| CD3-AF700 | Biolegend | Cat# 100216; RRID: AB_493697 |
| CD4-FITC | Biolegend | Cat# 100406; RRID: AB_312691 |
| CD8-BV510 | Biolegend | Cat# 100752; RRID: AB_2563057 |
| CD19-FITC | Biolegend | Cat# 152404; RRID: AB_2629813 |
| CD44-BV421 | Biolegend | Cat# 103040; RRID: AB_2616903 |
| CD45-PE | Invitrogen | Cat# 12-0451-82; RRID: AB_465668 |
| CD62L-APC | Biolegend | Cat# 104412; RRID: AB_313099 |
| CD69-PE-Cy7 | Invitrogen | Cat# 25-0691-82; RRID: AB_469637 |
| IgA-BV421 | BD Bioscience | Cat# 743292; RRID: AB_2741405 |
| Fc block CD16/CD32 | BD Bioscience | Cat# 553141; RRID: AB_394656 |
| Goat anti-mouse IgG (HRP) | Jacksom ImmunoResearch | Cat# 115-035-003; RRID: AB_10015289 |
| Goat pAb to mouse IgG1 (HRP) | abcam | Cat# ab97240; RRID: AB_10695944 |
| Goat pAb to mouse IgG2a (HRP) | abcam | Cat# ab97245; RRID: AB_10680049 |
| Goat pAb to mouse IgA (HRP) | abcam | Cat# ab97235; RRID: AB_10681186 |
| Goat anti-mouse IgA (Biot) | Southern Biotech | Cat# 1040-80; RRID: AB_2794374 |
| SARS-CoV-2 nucleocapsid antibody | GeneTeX | Cat# GTX635679; RRID: AB_2888553 |
| Goat pAb to Rb IgG (HRP) | abcam | Cat# ab205718; RRID: AB_2819160 |
| **Bacterial and virus strains** | | |
| SARS-CoV-2-KMS1/2020 | (Che et al., 2020) | https://pubmed.ncbi.nlm.nih.gov/33165503/ |
| SARS-CoV-2 (wild-type) Spike pseudovirus | SinoBiological | Cat# PSV001 |
| SARS-CoV-2 (B.1.351) Spike pseudovirus | SinoBiological | Cat# PSV008 |
| SARS-CoV-2 (B.1.617.2) Spike pseudovirus | SinoBiological | Cat# PSV011 |
| **Chemicals, peptides, and recombinant proteins** | | |
| 2′3′-cGAMP VacciGrade | Invivogen | Cat# vac-nacga23 |
| SARS-CoV-2 RBD protein | SinoBiological | Cat# 40592-V08H |
| SARS-CoV-2 S1 protein | SinoBiological | Cat# 40591-V08H |
| SARS-CoV-2 full length spike protein, S1+S2 ECD-his, SFL | SinoBiological | Cat# 40589-V08B1 |
| SARS-CoV-2 full length spike protein, S1+S2 (mutants) ECD-his, $SFL_{mut}$ | SinoBiological | Cat# 40589-V08H4 |
| SARS-CoV-2 N protein | SinoBiological | Cat# 40592-V08H |
| B.1.351 variant full length S protein | SinoBiological | Cat# 40589-V08B7 |
| B.1.351 variant N protein | SinoBiological | Cat# 40588-V07E9 |
| B.1.617.2 variant full length S protein | SinoBiological | Cat# 40589-V08B16 |
| B.1.617.2 variant N protein | SinoBiological | Cat# 40588-V07E29 |
| EndoFit Ovalbumin (OVA) | Invivogen | Cat# vac-pova-100 |

(*Continued on next page*)

*Continued*

| Reagent or resource | Source | Identifier |
|---|---|---|
| Fetal Bovine Serum | Corning | Cat# 35-081-CV |
| Bovine Serum Albumin | Solarbio | Cat# 9048-46-8 |
| Recombinant Murine GM-CSF | Peprotech | Cat #315-03 |
| 3,5,3′,5′-tetramethylbenzidine (TMB) | Solarbio | Cat# PR1200 |
| Peroxidase-conjugated streptavidin | Jacksom ImmunoResearch | Cat# 016-030-084; RRID: AB_2337238 |
| Collagenase D | Sigma | Cat# 110888866001 |
| DNase I | Sigma | Cat# 11284932001 |
| 7-AAD | BD Bioscience | Cat# 559925; RRID: AB_2869266 |
| BD Cytofix/Cytoperm | BD Bioscience | Cat# 554722; RRID: AB_2869010 |
| Perm/Wash Buffer | BD Bioscience | Cat# 554723; RRID: AB_2869011 |
| AEC Substrate | BD Bioscience | Cat# 551951; RRID: AB_2868954 |
| Trizol | Thermo Fisher | Cat # 15596026 |
| 10% neutral buffered formalin | Sigma | Cat# Z2902 |
| Ficoll-Paque PREMIUM | GE | Cat# 17544602 |
| PERCOLL | GE | Cat# 17089102 |
| **Critical commercial assays** | | |
| Mouse IFN-γ Elispot Kit | R&D systems | Cat# EL485 |
| Mouse IL-4 Elispot Kit | R&D systems | Cat# EL404 |
| RNeasy mini Kit | QIAGEN | Cat# 74104 |
| One Step PrimScript RT-PCR Kit | TaKaRa | Cat# RR064A |
| Firefly-Glo Luciferase Reporter Assay Kit | Dalian Meilun Biotechnology Co.Ltd. | Cat# MA0519 |
| Mouse IL-6 Elisa Kit | Novus Biologicals | Cat# VAL604 |
| Mouse TNF-α Elisa Kit | Novus Biologicals | Cat# VAL609 |
| Mouse IFN-β Elisa Kit | Novus Biologicals | Cat# VAL612 |
| Mouse IP-10 Elisa Kit | abcam | Cat# ab260067 |
| **Deposited data** | | |
| RNA-seq data | NCBI SRA | PRJNA780080 |
| **Experimental models: Cell lines** | | |
| Vero cells | World Health Organization (WHO) | N/A |
| ACE2 overexpressed 293T cells | Prof. WeiJin Huang (National Institutes for Food and Drug Control) | N/A |
| **Experimental models: Organisms/strains** | | |
| C57BL/6 wild type mice | Beijing Charles River Laboratory | N/A |
| Transgenic hACE2 mice (C57BL/6) | Shanghai Model Organisms Center, Inc. | Cat# NM-HU-200218 |
| **Oligonucleotides** | | |
| E protein-Probe: 5′-ACACTAGCCATCCTTACTGCGCTTCG-3′) | This paper | N/A |
| Primer of E protein gene Forward: (5′-ACAGGTACGTTAATAGTTAATAGCGT-3′) | This paper | N/A |
| Primer of E protein gene Forward: (5′-ATATTGCAGCAGTACGCACACA-3′) | This paper | N/A |
| **Software and algorithms** | | |
| Prism 8.0 | GraphPad | https://www.graphpad.com/scientific-software/prism/ |
| Microsoft Excel | Microsoft | https://www.microsoft.com/en-ww/microsoft-365/excel |
| BioSpot analyzer | Cellular Technology Limited | N/A |
| Flowjo v10 | TreeStar | https://www.flowjo.com/ |

(*Continued on next page*)

*Continued*

| Reagent or resource | Source | Identifier |
|---|---|---|
| Metascape web tool | (Zhou et al., 2019a) | https://metascape.org/gp/index.html#/main/step1 |
| Adobe Illustrator | Adobe Illustrator | https://www.adobe.com/ RRID:SCR_010279 |
| Adobe Photoshop | Adobe Photoshop | https://www.adobe.com RRID: SCR_014199 |
| Other | | |
| 96-well plates | Corning | Cat# 9018 |
| 96-well plates | Corning | Cat# 3590 |
| 96-well Filtration plates | Millipore | Cat# MSIPS4510 |
| 96-well opaque plates | JingAn biological science and Technology Co., Ltd. | Cat# J09601 |
| Dulbecco's Modified Eagle Medium (DMEM) | GIBCO | 11965-092 |
| Phosphate buffer saline (PBS) | GIBCO | 14190-144 |

## RESOURCE AVAILABILITY

### Lead contact

Further information and requests for resources and reagents should be directed to and will be fulfilled by the Lead Contact, Mingbo Sun (smb@imbcams.com.cn)

### Materials availability

All unique/stable reagents generated in this study are available from the Lead Contact with a completed Materials Transfer Agreement (MTA).

### Data and code availability

- The RNA-seq datasets generated during this study are available at the NCBI SRA (PRJNA780080). Additional supplemental items are available from Mendeley Data at: https://dx.doi.org/10.17632/9926fkjgs6.1.
- This paper does not generate original code.
- Any additional information required to reanalyze the data reported in this paper is available from the lead contact upon request.

## EXPERIMENTAL MODEL AND SUBJECT DETAILS

### Viruses and cells

The SARS-CoV-2 strain SARS-CoV-2-KMS1/2020 (GenBank accession number: MT226610.1), which was isolated from a human clinical sample collected at Yunnan Hospital of Infectious Diseases, was propagated in Vero cells obtained from the World Health Organization (WHO). Dulbecco's modified Eagle medium (DMEM) supplemented with 10% fetal bovine serum (FBS) and an antibiotic–antimycotic solution was used for cell culture. All experimental procedures involving SARS-CoV-2 were conducted in a BSL-3 laboratory. ACE2 overexpressed 293T cells lines were obtained from Professor WeiJin Huang from the Institute for Biological Product Control, National Institutes for Food and Drug Control, Beijing, China, and incubated in DMEM at 37°C and 5% $CO_2$.

### Mice and ethics statements

Specific pathogen-free (SPF) 6- to 8-week-old male and female C57BL/6 mice were purchased from Beijing Charles River Laboratory (Beijing, China). SPF 6- to 8-week-old male and female hACE2 Tg mice (half male and half female) which expressed ACE2 and were generated on the C57BL/6 background, were obtained from Shanghai Model Organisms Center, Inc. All mice used in this study were treated in accordance with the Guide for the Care and Use of Laboratory Animals of the People's Republic of China. All protocols were reviewed and approved by the Committee on the Ethics of the Institute of Medical Biology, Chinese Academy of Medical Sciences (IMBCAMS; Assurance numbers: DWSP202008022 and DWSP202011005). Animals were bred and maintained under SPF conditions at IMBCAMS at a constant temperature (20–24°C) and humidity (45%–65%) with lighting on a fixed light/dark cycle (12-h/12-h). Animals were humanely euthanized after reaching a humane endpoint. All animal studies involving SARS-CoV-2 were performed in the biosafety level 3 (BSL-3) laboratory.

## METHOD DETAILS

### Isolation and stimulation of dendritic cells

Bone marrow-dendritic cells (BMDCs) were isolated from mouse bone marrow cells as previously described. Briefly, bone marrow cells were isolated and cultured in RPMI 1640 medium containing 20 ng/mL recombinant GM-CSF (Peprotech), 100 U/mL penicillin, 100 μg/mL streptomycin, and 10% FBS. Petri dishes containing $2 \times 10^6$ cells in 10 mL were incubated at 37°C in 5% $CO_2$. At day 3 of incubation, a further 10 mL of fresh complete medium with GM-CSF was added, and 10 mL of medium was replaced with fresh supplemented medium containing GM-CSF on days 6. Immature BMDCs were collected on day 7 for further experiments. The BMDCs were treated with KF (4 μg/mL), cGAMP (4 μg/mL) alone, or combination of SF (4 μg/mL) and cGAMP (4 μg/mL) *in vitro* for 24 h. Cells were treated with lipopolysaccharide (LPS, 1 μg/mL) or sterile PBS as positive and negative controls, respectively. Cytokines (IP-10, TNF-α, IFN-β, and IL-6) levels in the supernatant were quantified by ELISA. The stimulated BMDCs were stained with the specific antibodies and analyzed by using FlowJo software.

### Vaccine formulations

The antigens used in experimental vaccines, including the N protein (N), full-length SARS-CoV-2 S protein (SFL), $SFL_{mut}$, S1 subunit (S1), and RBD, were obtained from Sino Biological Inc (China). The adjuvant cGAMP was purchased from InvivoGen (San Diego, USA). A nonpathogenic *E. coli*-derived flagellin (KF) plasmid was a generous gift from Dr. Yan Huimin (Wuhan Institute of Virology, Chinese Academy of Sciences). The construction of pET28a carrying KF and the associate KF expression were described in a previous study (Sun et al., 2012). The different SARS-CoV-2 antigens mentioned above were used at a dose of 8 μg/mouse for vaccination. cGAMP and KF (4 μg/mouse) were used as adjuvants.

A reference inactivated SARS CoV-2 vaccine was prepared by the IMBCAMS as described in a previous study (Che et al., 2020). Briefly, the SARS-CoV-2 strain KMS-1 (GenBank accession number: MT226610.1) was cultured in Vero cells. The virus was inactivated with formaldehyde at a dilution of 1:4000 for 48 h. It was further purified through column chromatography and concentration. Then, beta-propiolactone was added for further inactivation, followed by a second purification via the same protocol mentioned above. The inactivated vaccine was prepared with 100 enzyme-linked immunosorbent assay (ELISA) units (EU), absorbed with 0.25 mg $Al(OH)_3$ adjuvant and suspended in 0.2 mL of PBS for each dose.

### Mouse experiments

For the initial adjuvant evaluation experiment, 6-8 weeks old C57BL/6 mice were intranasally immunized on days 0, 14 and 28 with ovalbumin protein (OVA, 20 μg per dose) alone or OVA protein admixed with KF (4 μg per dose), cGAMP (4 μg per dose), or KF (4 μg per dose) plus cGAMP (4 μg per dose) in a total volume of 30 μL. Control mice were administered phosphate buffered saline (PBS). Mice were euthanized at day 14 after last immunization.

For screening the optimal antigen, 6- to 8-week-old C57BL/6 mice were intranasally immunized with 30 μl of different experimental vaccines or PBS three times with two-week intervals after anaesthetization with isoflurane (Figure 2A). Briefly, four groups were intranasally immunized with the N protein (8 μg/dose) and different forms of the S protein (RBD, S1, SFL, or $SFL_{mut}$; 8 μg/mouse) formulated with KF (4 μg/dose) and cGAMP (4 μg/dose). One group of mice was immunized with PBS to establish a control group. Two weeks after the final immunization, blood was collected and left on ice for 30 min; serum was then collected by centrifugation at 3000 × g for 10 min at 4°C. Nasal wash (NW) was collected in 200 μL of PBS. Bronchoalveolar lavage fluid (BALF) was collected in 1 mL of PBS. All samples were stored at −80°C until used.

For evaluating the immunogenicity of candidate vaccine, 6- to 8-week-old C57BL/6 mice mice were given with $SFL_{mut}$ and N protein supplemented with or without combined adjuvant via intranasal route (IN) three times with two-week intervals. These groups were compared to a reference vaccine which is knew to be protective: an inactivated vaccine using whole virus administered intraperitoneally (IP) twice with four-week intervals. Additionally, to determine if the effects of combined adjuvant was dependent by immunization route, thus mice were immunized with IP delivered $SFL_{mut}$ and N protein combined with KF and cGAMP. And mice IN administered PBS as placebo group (Figure 3A). Control mice were administered PBS. Mice were euthanized at day 14 after last immunization.

For evaluation of candidate vaccine protective-efficacy, 6- to 8-week-old hACE2 Tg mice were randomly allocated into three groups. The mice in the candidate vaccine group and the placebo group were intranasally vaccinated with 30 μl of candidate vaccine or 30 μl of PBS, respectively, three times at two-week intervals, while the mice in the reference inactivated vaccine group were intraperitoneally (IP) immunized with 200 μL of inactivated vaccine twice at 4-week intervals as a vaccine control (Figure 5A). All mice were anaesthetized with isoflurane before vaccination. After immunization, all hACE2 Tg mice were challenged with the wild-type SARS-CoV-2 strain KMS-1 (GenBank accession number: MT226610.1) in the BSL-3 laboratory. Mice were anaesthetized with isoflurane and intranasally inoculated with $10^3$ plaque-forming units (PFU) of SARS-CoV-2. The nasal washes (NW) and throat swab were collected daily, and the body weight and survival of each mouse were also monitored daily. Animals in each group were euthanized at day 2, 5, and 7 post infection (dpi) to collect tissues. When mice were unable to eat or stand or had lost more than 20% of their body weight, euthanasia was performed.

### Enzyme linked immunosorbent assay

ELISA plates were coated overnight at 4°C. The coating buffer was aspirated, and the wells were blocked with 200 μL of 1X PBS + 0.05% Tween-20 + 3% BSA (PBST-3% BSA) for 2 h at 37°C. Samples were diluted in PBST-1% BSA in a separate 96-well polypropylene plate. The plates were washed four times with PBST, followed by the addition of 50 μL of serum dilutions (PBST-1% BSA) and incubation for 1 h at 37°C. Following washing, 50 μL of anti-mouse IgG, IgG1, IgG2a and/or IgA-horseradish peroxidase conjugates was added to each well. After 1 h of incubation at 37°C, the plates were again washed four times with PBST, and 100 μL of 3,5,3′5′-tetramethylbenzidine TMB was added. Following a 10- to 20-min incubation, reactions were stopped with 50 μL of 2 M sulfuric acid. The absorbance of plates at 450 nm was read. Endpoint titers were determined as the dilution that exhibited an optical density exceeding $\geq$ 2.1 times the background level (secondary antibody alone). Cytokines from the supernatants of BMDC cultures Elisa assays was performed according to the manufacturer's instructions.

### SARS-CoV-2 neutralization assay

The neutralizing activity of serum from vaccinated mice against wild-type SARS-CoV-2 *in vitro* was evaluated with Vero cells. Heat-inactivated serum was serially diluted 2-fold in 96-well plates, and 50 μL of live SARS-CoV-2 (100 cell culture infectious dose 50% (CCID50)/well) was added to 50 μL of each serum dilution and incubated for 2 h at 37°C/5% $CO_2$ in a humidified incubator. Subsequently, the mixture was transferred to Vero cells in a 96-well plate, and the samples were evaluated in duplicate. After incubation for 5 days at 37°C/5% $CO_2$, the cytopathic effects (CPEs) were recorded to determine the NAb titer. The geometric mean titers (GMTs) of NAbs were measured. Antibody titers $\geq$ 4 was considered positive.

### Enzyme-linked immunospot assay

T cell detection by IFN-γ and IL-4 ELISpot assays was performed according to the manufacturer's instructions. Briefly, precoated 96-well plates were seeded with 5 μg/ml specific stimulants and 4 × $10^5$ mouse splenocytes or pneumonocytes in a total volume of 100 μL and incubated. Following a 24-h incubation at 37°C/5% $CO_2$, the cells were removed, and an anti-IFN-γ or anti-IL-4 detection antibody was added, followed by addition of streptavidin-ALP. For specific IgA-secreting cells detection, MultiScreen filter 96-well plates were pre-coated with 5 μg/well of specific protein overnight at 4°C. After rinsing with PBS, plates were blocked for 30 min at room temperature with culture medium. Single cell suspensions of splenocytes or pneumonocytes were added to the coated plates and incubated at 37°C/5% $CO_2$ for 24 h. After washing with PBS, plates were incubated with biotinylated anti-IgA followed by incubation with streptavidin conjugated horseradish peroxidase, each for 1 h at room temperature. After additional washes with PBS, AEC substrate solution was added for spot development. The reaction was stopped by rinsing with water. Spots were developed using BCIP/NBT and analyzed by a Cellular Technology Limited (CTL) ELISpot reader.

### Detection of lung tissue-resident cells

To discriminate circulating cells from lung-resident cells, we employed a well-described approach in which mice were intravenously (i.v.) administered an anti-mouse CD45 PE-conjugated antibody 10 min before euthanasia, and then the lungs were harvested (Anderson et al., 2014). Circulating cells were exposed to the antibody and labeled as CD45+, whereas lung-localized cells remained CD45-.

### Flow cytometry

Single cell suspensions were obtained from BMDCs or tissues. Nasal-associated lymphoid tissues (NALTs) and lungs were minced and digested with collagenase D (1 mg/ml; Roche) and DNase I (20 U/ml; Roche) for 45 min at 37°C on a shaker. Next, the NALTs were passed through a 70-μm cell strainer to obtain single-cell suspensions. For cell preparation from the lungs, tissues were passed through a 70-μm cell strainer, washed twice in complete RPMI 1640 medium, mixed with 40% Percoll and loaded onto a 70% Percoll layer for isolation of mononuclear cells according to the manufacturer's instructions. Cells were incubated with anti-CD16/CD32 Fc block. Then, the cells were incubated with 7-AAD (BD Bioscience), followed by surface staining with fluorochrome-conjugated anti-mouse antibodies for the following markers. For intracellular cytokine staining, cells were first stained with 7-AAD and an antibody specific for a surface marker. After washing twice, the cells were fixed and permeabilized with Cytofix/Cytoperm and then stained intracellular marker. All samples were acquired on a flow cytometer (Beckman), and data were analyzed with FlowJo software (TreeStar).

### RNA-seq

The nasal mucosa and/or NALT were collected on day 14 after the last immunization and homogenized with TRIzol reagent, and total RNA was extracted with chloroform/isopropanol, followed by purification using the RNeasy Mini Kit (QIAGEN). The raw reads generated for the nasal mucosa or NALT were filtered by SOAPnuke software (Cock et al., 2010), which proceeded by removing adaptor-polluted reads, reads with unknown sequences "N" accounting for more than 5% of the reads, and low-quality reads defined using parameters such as average base content per read and GC distribution in the read. The clean reads were mapped on the reference Mus-musculus_GRCm38.p6 using hierarchical indexing for spliced alignment of transcripts (HISAT) software v2.1.0 (Kim et al., 2015). The sequencing data generated during this study are available at the NCBI SRA archive (PRJNA780080). Differentially expressed genes (DEGs) were filtered with DESeq2 (Love et al., 2014) using the thresholds of a false discovery rate (FDR) of 5%

and an absolute fold change of 2 to determine the final lists. Heatmap illustrator (heml) software was applied to generate heatmaps. Enrichment analysis of the functions of the DEGs was conducted using the Metascape web tool (Zhou et al., 2019a) (https://metascape.org/gp/index.html#/main/step1). Gene sets were derived from the Gene Ontology (GO) Biological Process (GO-BP) ontology.

### Measurement of viral burden

Viral RNA in nasal, pharyngeal, and peripheral blood samples was extracted using TRIzol reagent (Tiangen, China) following vortexing. Total viral RNA in tissues was extracted by mechanical homogenization with iron beads. RNA was eluted in 30 μL of elution buffer and used as a template for qRT-PCR. Two SARS-CoV-2 RNA standards were generated for transcription by E protein regions transcribed *in vitro* (E protein-F: 5′-ACAGGTACGTTAATAGTTAATAGCGT-3′; E protein-R: 5′-ATATTGCAGCAGTACGCACACA-3′; E protein-P: 5′-ACACTAGCCATCCTTACTGCGCTTCG-3′). Two microliters of RNA were used to quantify viral RNA copies with the One Step PrimeScript™ RT-PCR Kit (Takara, China) according to the manufacturer's instructions. The amplification procedures were set up on a Bio-Rad instrument as follows: 42°C for 5 min and 95°C for 10 s followed by 39 cycles consisting of 95°C for 5 s, 60°C for 30 s, and a default melting curve step. A standard curve was generated using 10-fold dilutions of SARS-CoV-2 RNA standard produced by *in vitro* transcription. Assay sensitivity was 50 copies/100 μl. Viral loads were calculated as the genome copies of SARS-CoV-2 in 1 mL swab elutes/NW or in 1 mg of tissue.

### Virus titration

Quantitation of live infectious virus by a CCID50 assay was performed for nasal turbinate, lung, and brain tissues. Briefly, Vero cells in a 96-well plate ($2 \times 10^4$ cells/well, duplicate) were inoculated with 10-fold serial dilutions of supernatants from organ homogenates. The mixtures were performed in duplicate, and the plate was incubated for 5 days at 37°C in a humidified 5% CO2 incubator. The CPEs were recorded to determine the organ homogenate virus titers. Viral titers were calculated as $CCID_{50}$/mL.

### Histopathology and immunohistochemistry

For histopathologic analysis, tissues (brain, nasal turbinate and lung) from necropsied mice were fixed in 10% formalin, embedded in paraffin, and sectioned at 3-5 μm. The sections were stained with hematoxylin and eosin (H&E). For immunohistochemistry, the SARS-CoV-2 N protein was detected using the monoclonal antibody HL344 (GeneTex, China). Sections were incubated with the rabbit antibody specific for the N antigen of SARS-CoV-2 for 1 h after heat-induced epitope retrieval. Antibody labeling was visualized by development with DAB. Digital images were captured and evaluated with a histological section scanner (Aperio Digital Pathology, Leica).

### Pseudovirus neutralization assay

For pVNT experiments, serial 3-fold diluted serum, starting at 1:30, were incubated with S protein bearing pseudotype particles for 1 hour at 37°C, before the mixtures were inoculated onto ACE2 overexpressed 293T cells. In all cases, particles incubated only with medium served as control. The supernatant was then removed, and luciferase substrate was added to each well, followed by incubation for 5 min in darkness at room temperature. Luciferase activity was then measured using Thermo scientific Varioskan Flash. The 50% pseudovirus neutralization ($pVNT_{50}$) of the serum samples, which indicates the plasma dilution that causes a 50% reduction of entry efficiency, were determined by luciferase activity 48 h after exposure to the virus-serum mixture with four-parameter non-linear regression inhibitor curve in GraphPad Prism 8.0.

## QUANTIFICATION AND STATISTICAL ANALYSIS

Results are presented as the means ± the SEM and were analyzed with GraphPad Prism 8.0 software. An unpaired two-sided Student's t test was utilized to determine statistical significance between two groups. One-way ANOVA with Tukey's post hoc test was employed to assess differences among multiple groups. *$p < 0.05$, **$p < 0.01$, ***$p < 0.001$. The details on the statistical test and the error bars are specified in the figure legends.